

國立交通大學

機械工程學系  
碩士論文

Plasma Assisted Catalytic System for Ethanol Steam Reforming-  
Comparison of Different Catalysts

利用滑動電弧的電漿輔助觸媒進行自熱反應重組乙醇的研究：  
不同觸媒的比較

研究生：沈育安

指導教授：吳宗信 博士

二零一二年七月

利用滑動電弧的電漿輔助觸媒進行自熱反應重組乙醇的研究：

不同觸媒的比較

**Plasma Assisted Catalytic System for Ethanol Steam Reforming-  
Comparison of Different Catalysts**

學生：沈育安

指導教授：吳宗信 博士

Student : Yu-An Shen

Advisor : Dr. Jong-Shinn Wu

國立交通大學

機械工程學系

碩士論文

A Thesis

Submitted to Department of Mechanical Engineering

National Chiao Tung University

In Partial Fulfillment of the Requirements

For the Degree of

Master of Science

In

Mechanical Engineering

July 2012

Hsinchu, Taiwan

二零一二年七月

# 利用滑動電弧的電漿輔助觸媒進行自熱反應重組乙醇的研究：

## 不同觸媒的比較

學生：沈育安

指導教授：吳宗信 博士

國立交通大學機械工程學系

### 摘要

本實驗探討利用滑動電弧的電漿輔助觸媒經過自熱反應的方式重組乙醇存並進行產生氫氣之研究。而滑動電弧的電漿可以由一個能夠產生 20kHz 的電源供應器來提供所需的功率。其中，在電漿輔助觸媒生產氫氣的過程搭配兩種不同種類的觸媒，分別是貴重金屬 Rh 的觸媒和非貴重金屬  $\text{Ni}_{0.35}\text{Mg}_{2.65}\text{FeO}_{4.5}$  的觸媒，藉由這兩者去比較滑動電弧搭配觸媒各有怎樣的 effects。首先在探討貴重金屬中，藉由成分為 5 wt% Rh/CeO<sub>2</sub>/Al<sub>2</sub>O<sub>3</sub> 的觸媒，並在空氣流量 0.5-2.0 SLM 中，使乙醇水氣重組。在觸媒重組的實驗結果中，當氣體流量為 1.0 SLM 時，氣體轉換率達到 100%，氫氣選擇比也達到最高的 115%，但流量為較低的 0.5slm 和較高的 1.5slm 時，氫氣選擇比分別為 95% 和 70% 的選擇比。加入電漿輔助觸媒後，可以明顯地看到在 1.0 SLM 及 1.5 SLM 時，氫氣選擇比分別為 113% 和 111%。由此結果可以看出，PAC 的系統在較高流量時，仍然可以藉由目前設備達到較好的氫氣選擇比。然而當流量在達到更高的 2.0 SLM 時，氫氣的選擇比急速的下降至 70% 上下並且和觸媒的氫氣選擇比幾乎一樣，可能的原因是，電漿處理氣體的停留時間

下降，使得大部分的氣體僅藉由觸媒反應產生重組。

而在非貴重金屬的探討中，使用成分為 10 wt%  $\text{Ni}_{0.35}\text{Mg}_{2.65}\text{FeO}_{4.5}/\text{Al}_2\text{O}_3$  的觸媒使酒精重組並產生氫氣。而結果顯示出，當空氣流量在 1 SLM，觸媒溫度為 400 °C 時，觸媒可產生出最高的氫氣選擇比大約 55%，還有的乙醇轉換效率接近 100%，並且隨著溫度下降而下降。在經過電漿輔助後，氫氣選擇比可以來到約 75%。但即使氫氣選擇比有提升，但是乙醇的轉換效率卻大幅下降至 73 % 並且氫氣選擇比仍然遠低於搭配貴重金屬的選擇比。而最有可能的原因是， $\text{Ni}_{0.35}\text{Mg}_{2.65}\text{FeO}_{4.5}$  本身「水氣轉換氫氣」的這項反應式是幾乎不會發生的，對於氫氣的選擇比以及乙醇轉換效率會大幅下降有很好的解釋。而上述所解釋的現象和氣體成分詳細的分析皆可透過經由氣體層析儀得知。





# Plasma Assisted Catalytic System for Ethanol Steam Reforming- Comparison of Different Catalysts

Student : Yu-An Shen

Advisor : Dr. Jong-Shinn Wu

Department of Mechanical Engineering  
National Chiao Tung University

## Abstract

In this study, the preheated ethanol steam flow is reformed using a gliding-arc plasma-assisted catalyst (PAC) system with a power frequency of 20 kHz. Among the PAC reforming, the noble catalyst Rh and non-noble catalyst  $\text{Ni}_{0.35}\text{Mg}_{2.65}\text{FeO}_{4.5}$  respectively is used to compare PAC with catalyst alone reforming by generating the hydrogen selectivity and conversion rate via different experimental parameters. In Rh catalyst alone reforming at the range of air flow rates of 0.5-2.0 SLM, the results show that a 100% conversion rate and a maximum of 115% hydrogen selectivity could be obtained at a C/O ratio of 0.7 with an air flow rate of 1.0 SLM. However, hydrogen selectivity decreases rapidly to 95% and 70% at lower (0.5 SLM) and higher (1.5 SLM) air flow rates, respectively. With the addition of a gliding arc prior to the catalyst, hydrogen selectivity reaches 113% and 111% at air flow rates of 1.0 and 1.5 SLM, respectively, with a plasma absorption power of approximately 200 W. This shows that very high hydrogen selectivity (>110%) can be obtained at air flow rates of both 1.0 and 1.5 SLM under the current experimental setup.

However, at a 2.0 SLM air flow rate, the hydrogen selectivity of PAC drops down to 70% and is almost the same as that for reforming with the catalyst alone. The above observations correlate strongly with the residence time of the gas flow in plasma with the catalyst. In the  $\text{Ni}_{0.35}\text{Mg}_{2.65}\text{FeO}_{4.5}$  catalyst reforming at the range of catalyst temperatures of 200-400°C, the highest hydrogen selectivity (~55%) and conversion rate are close the 100% at temperature 400 °C and drop down rapidly with decreasing the temperature. However, the PAC with  $\text{Ni}_{0.35}\text{Mg}_{2.65}\text{FeO}_{4.5}$  catalyst can improve the selectivity of catalyst alone reforming to 75% at the temperature 400°C. Even though the selectivity could be raised, the conversion drop down to 73% and hydrogen selectivity is much lower than PAC with Rh catalyst. The reason maybe the plasma generates a lot of  $\text{H}_2\text{O}$  but the catalyst is inefficient at water-gas-shift (WGS) chemical reaction equation, as estimated using measurements of the gas composition from gas chromatography.

## 誌謝

首先非常誠摯的感謝親愛的指導教授吳宗信博士，在教授細心的指導下，使我在電漿領域的研究上，有著相當的了解並完成這篇論文，過程中不時的討論並指點我正確的方向，使我能在碩士班兩年中對於做研究方法和做研究精神有著很大的躍進，而老師對學問的嚴謹和做事的方態度更是成為晚輩學習的典範。本論文的完成另外得要感謝口委交大的陳慶耀教授、劉耀先教授及台大的廖國基教授，因為有你們的建議及意見，使得本論文能夠更完整而嚴謹。在實驗所需的資金方面，感謝國科會淨煤計畫 (NSC 101-3113-P-009 -002) 和教育部特色計畫給予很大的協助以及交通大學在人才的培養方面給予很大的支持

兩年來的學習，在研究室裡共同的生活點滴，學術上的討論、做研究的精神、對於社會的認識以及對於團隊的合作，都要感謝眾位學長姐、同學、學弟妹的指教。其中包括電漿實驗組的宜偉哥、志東、志華、駿平和國淳，特別是駿平在我實驗上的幫助尤其之多，讓我猶記在心；在模擬組方面，包括了燦哥、蘇正勤學長、凱文哥、邱沅明學長、昆模哥、古必哥、孟華和雅茹學姐、子豪哥及冠融哥，其中在網絡給予我相當大協助的古必哥，在自控方面的冠融哥，特別感謝他們的協助；感謝我們的助理王姊和劉小姐給予我很多的幫忙；已經畢業的偉能哥、綠豆學長及柏村哥，其中特別感謝將我訓練得很好的偉能哥；還要謝謝同學阿康和魏世昕互相的學習和幫助。很榮幸能和以上這麼多優秀的人共事過。

最後謝謝遠在高雄的家人，謝謝他們對於我在課業上給予最大的支持和力量，也很感謝他們能體會我因為距離、時間、金錢和課業，所以無法常常回去和他們想處。未來希望自己的所學，能為社會盡一份力。

最後將此文我最親愛的雙親

# Table of Contents

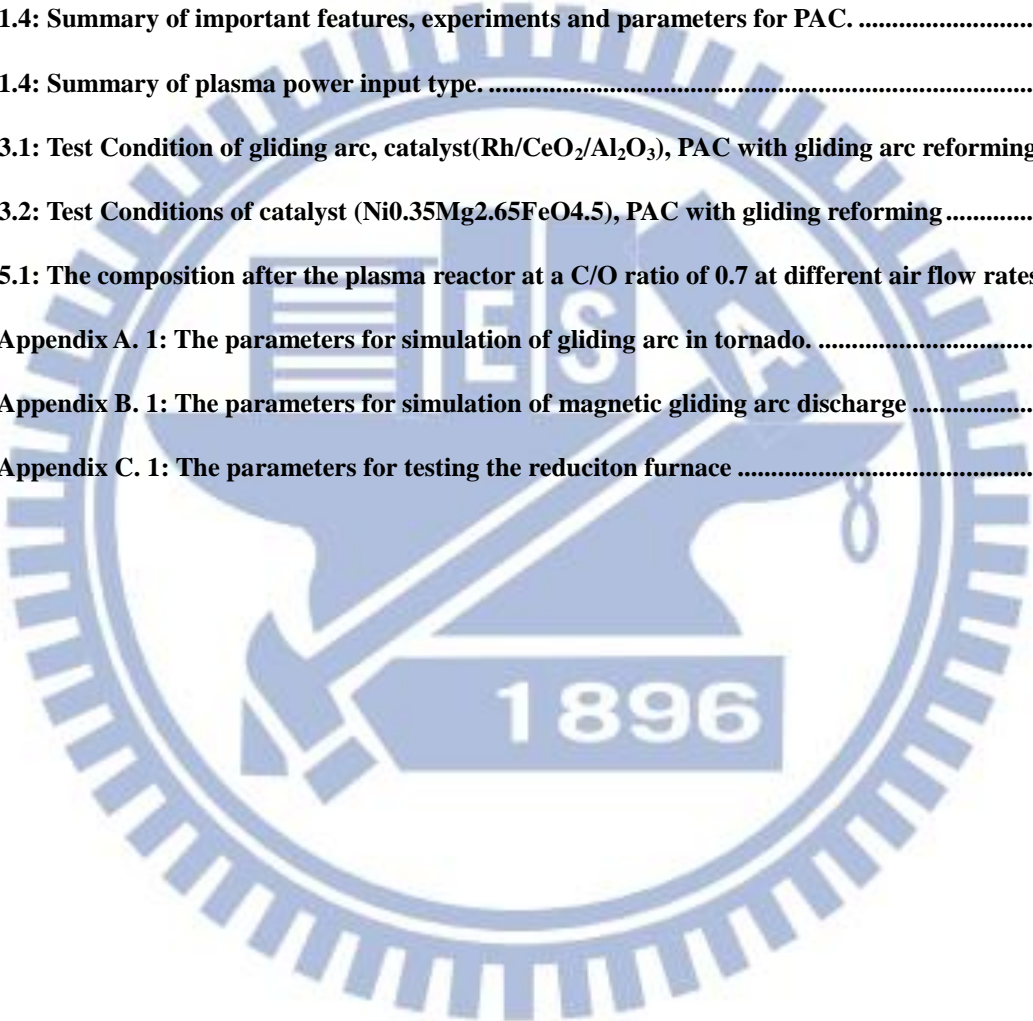
摘要.....	I
Abstract.....	III
誌謝.....	V
Table of Contents.....	VI
List of Tables.....	VIII
List of Figure.....	IX
Nomenclature.....	XII
<b>Chapter 1 Introduction .....</b>	<b>1</b>
1.1 BACKGROUND AND MOTIVATION .....	1
1.1.1 Hydrogen Energy Production .....	1
1.1.2 Overview of Reforming Technologies .....	3
1.1.3 Plasma Reforming Technologies.....	6
1.1.5 Hydrocarbon Reforming Fuel .....	8
1.1.6 Literature Survey .....	9
1.2 SPECIFIC OBJECTIVES OF THIS THESIS.....	11
<b>Chapter 2 Theoretical Method .....</b>	<b>13</b>
2.1 THEORETICAL ANALYSIS.....	13
2.1.1 The Physical Phenomenon of Gliding-Arc.....	13
2.1.2 Chemical Reaction Paths of Ethanol Reforming .....	14
2.1.3 Definition of Several Performance Parameters .....	15
<b>Chapter 3 Experimental Methods.....</b>	<b>17</b>
3.1 OVERVIEW OF EXPERIMENTAL SETUP .....	17
3.2 EXPERIMENTAL FACILITIES .....	18
3.2.1 Plasma Reactor .....	18
3.2.2 AC Power Supply and Pulse Generator .....	18
3.2.3 Fuel Feeding and Heating System .....	19
3.2.4 Catalyst Preparation.....	20
3.2.4.1 Rh/CeO <sub>2</sub> /Al <sub>2</sub> O <sub>3</sub> .....	20
3.2.4.2 Ni <sub>0.35</sub> Mg <sub>2.65</sub> FeO <sub>4.5</sub> /Al <sub>2</sub> O <sub>3</sub> .....	21
3.3 EXPERIMENTAL INSTRUMENTATION .....	21



3.4 EXPERIMENTAL PROCEDURES.....	22
3.4.1 Catalytic Reforming.....	22
3.4.2 Plasma Reforming .....	22
3.4.3 Plasma Assisted Catalytic Reforming .....	22
3.5 TEST CONDITIONS .....	23
<b>Chapter 4 Characterization of Gliding Arc Plasma .....</b>	<b>24</b>
4.1 VISUALIZATION .....	24
4.2 ELECTRICAL PROPERTIES .....	24
<b>Chapter 5 Results and Discussion .....</b>	<b>25</b>
5.1 REFORMING WITH GLIDING ARC PLASMA .....	25
5.1.1 Effect of C/O ratio.....	25
5.1.2 Effect of Gas Flow Rate .....	25
5.2 CATALYST REFORMING.....	26
5.2.1 Rh.....	27
5.2.2 Ni <sub>0.35</sub> Mg <sub>2.65</sub> FeO <sub>4.5</sub> /Al <sub>2</sub> O <sub>3</sub> .....	28
5.3 PLASMA ASSISTED CATALYST (PAC) REFORMING .....	28
5.3.1 PAC reforming with Rh catalyst.....	29
5.3.2 PAC reforming with Ni <sub>0.35</sub> Mg <sub>2.65</sub> FeO <sub>4.5</sub> Catalyst .....	30
<b>Chapter 6 Conclusion and Future Work .....</b>	<b>31</b>
6.1 CONCLUSION.....	31
6.2 RECOMMENDATIONS FOR FUTURE WORK .....	33
<b>References .....</b>	<b>34</b>
<b>Appendix A. Discussion of Gliding Arc in Tornado (GAT) .....</b>	<b>42</b>
<b>Appendix B. Discussion of Magnetic Gliding Arc Discharge (MGAD) .....</b>	<b>44</b>
<b>Appendix C. Hydrogen Reduction Furnace .....</b>	<b>45</b>

## List of Tables

Table 1.1: Properties of ethanol steam reforming with different noble metal catalysts. ....	46
Table 1.2: Properties of ethanol steam reforming with different non-noble metal catalysts.....	47
Table 1.3: Summary of important features, experiments and parameters for plasma alone reforming. ....	48
Table 1.4: Summary of important features, experiments and parameters for PAC. ....	49
Table 1.4: Summary of plasma power input type. ....	50
Table 3.1: Test Condition of gliding arc, catalyst(Rh/CeO <sub>2</sub> /Al <sub>2</sub> O <sub>3</sub> ), PAC with gliding arc reforming.....	51
Table 3.2: Test Conditions of catalyst (Ni <sub>0.35</sub> Mg <sub>2.65</sub> FeO <sub>4.5</sub> ), PAC with gliding reforming.....	51
Table 5.1: The composition after the plasma reactor at a C/O ratio of 0.7 at different air flow rates. ....	52
Table Appendix A. 1: The parameters for simulation of gliding arc in tornado. ....	53
Table Appendix B. 1: The parameters for simulation of magnetic gliding arc discharge.....	54
Table Appendix C. 1: The parameters for testing the reduciton furnace.....	55



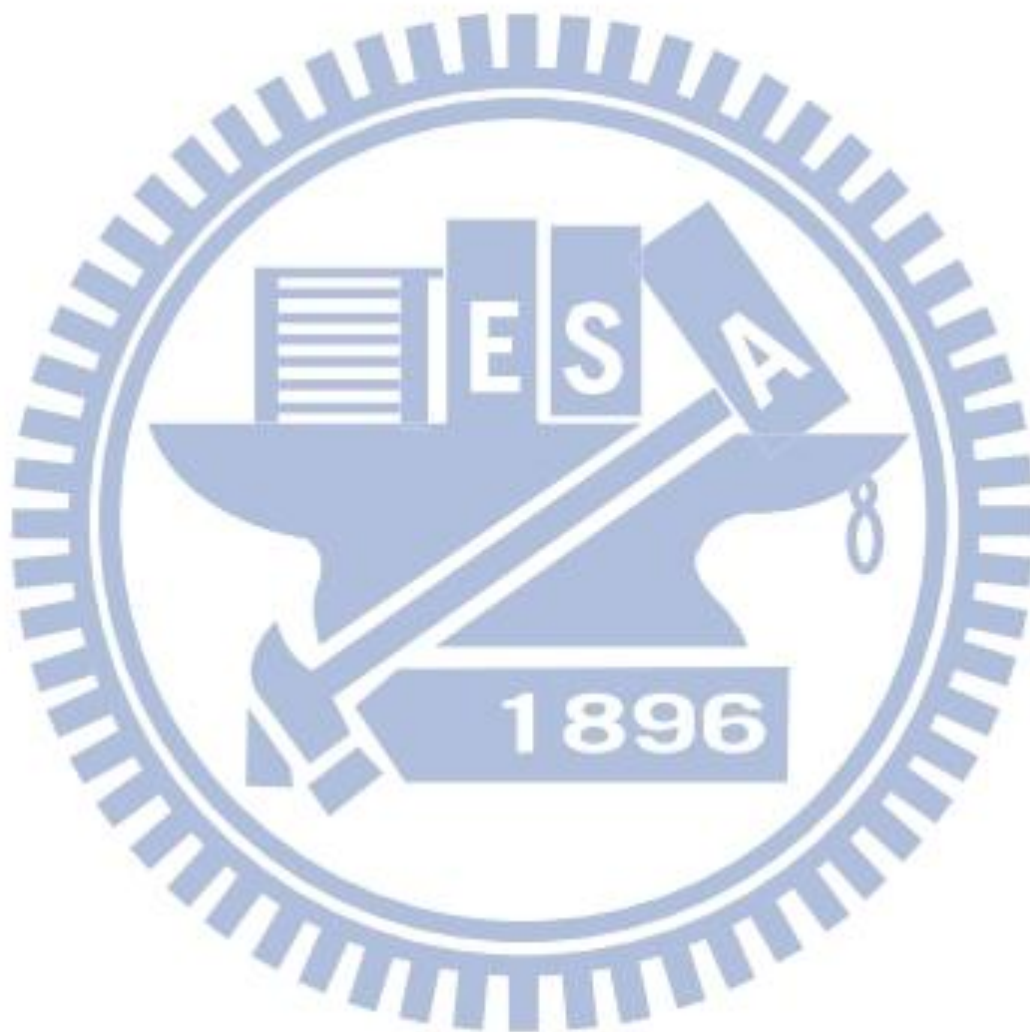
## List of Figure

Figure 1.1: Sketch of the typical test arrangement for ethanol reformer (left) and the SOFC (right) at CGET of NCTU. ....	56
Figure 1.2: The basic reaction of ethanol steam reforming [Vizcaino <i>et al.</i> , 2007]. ....	56
Fig. 1.3: Comparisons of yields for non-thermal (new plasmatron) and thermal (old plasmatron) plasmas [G. Petipas, <i>et al.</i> , 2007]. ....	57
Fig. 1.4: The comparison between different plasma reactors [G. Petipas, <i>et al.</i> , 2007].....	57
Figure 1.5: An energy diagram indicating the standard enthalpy ( $\Delta H^\circ$ ) and free energy changes ( $\Delta G^\circ$ ) in kJ/mol for the reactions in a renewable energy cycle operating between CO <sub>2</sub> and biomass [L. D. Schmidt, <i>et al.</i> , 2004].....	58
Figure 1.6: Typical arrangement of instrumentation for PAC system [Y. C. Yang <i>et al.</i> , 2009].....	58
Figure 2.1: Schematic of gliding arc reactor. [A. Fridman <i>et al.</i> , 2002]. ....	59
Figure 2.2: (a) voltage waveform of gliding arc production; (b) current waveform of gliding arc production [Antonius I. <i>et al.</i> , 2006]. ....	60
Figure 3.1: The experimental arrangement of PAC system. ....	60
Figure 3.2: Gas Chromatograph. ....	61
Figure 3.3: The self-designed gliding arc reactor. ....	62
Figure 3.4: PVM500 plasma driver.....	62
Figure 3.5: The MFC and liquid pump.....	63
Figure 3.6: The fuel Injections.....	63
Figure 3.7: The furnaces for heating system .....	64
Figure 3.8: The Rh catalyst setup procedure. ....	64
Figure 3.9: The Ni <sub>0.35</sub> Mg <sub>2.65</sub> FeO <sub>4.5</sub> catalyst setup procedure .....	65
Figure 3.9: High-voltage probe.....	65
Figure 3.10: Rogowski coil and Oscilloscope.....	66
Figure 4.1: The visualization of gliding arc discharge. The parameters: air flow rate is 1..5 SLM; The plasma power from power supply is 223 W with 20 kHz .....	67
Figure 4.2: The visualization of comparison of the gliding arc with C/O ratio or not.....	68

Figure 4.3: The electrical properties- I-V wave form.....	69
Figure 5.1: The conversion rate, $S_{H_2}$ and $S_{CO_2}$ versus the C/O ratio with plasma alone. ....	70
Figure 5.2: The conversion rate, $S_{H_2}$ and $S_{CO_2}$ as functions of the air flow rate with plasma alone at a C/O ratio of 0.7. ....	71
Figure 5.3: $S_{H_2}$ , $S_{H_2O}$ and $S_{CH_4}$ as functions of the air flow rate with plasma alone at a C/O ratio of 0.7.....	72
Figure 5.4: $S_{CO_2}$ , $S_{CO}$ and $S_{CH_4}$ as functions of the air flow rate with plasma alone at a C/O ratio of 0.7. ...	73
Figure 5.5: The conversion rate, hydrogen selectivity and carbon dioxide selectivity as functions of the air flow rate with catalyst alone. ....	74
Figure 5.6: The conversion rate, hydrogen selectivity and carbon dioxide selectivity as functions of the catalyst temperature with catalyst alone. ( $Ni_{0.35}Mg_{2.65}FeO_{4.5}$ ) .....	75
Figure 5.7: The conversion rate, hydrogen and carbon dioxide selectivity as a function air flow rate for the cases of PAC with Rh catalyst. ....	76
Figure 5.8: The comparison of conversion rate between catalyst reforming and PAC reforming using $Ni_{0.35}Mg_{2.65}FeO_{4.5}$ catalyst.....	77
Figure 5.9: The comparison of hydrogen selectivity between catalyst reforming and PAC reforming using $Ni_{0.35}Mg_{2.65}FeO_{4.5}$ catalyst.....	78
Figure Appendix A. 1: GAT system in a cylindrical (a) a cross-sectional view (b) Top view of swirl generator [Alexander Fridman, 2009]. ....	79
Figure Appendix A. 2: The vector in air flow rate (a). The injection of vector in $0^\circ$ injected angle (b). The injection of vector in $30^\circ$ injected angle .....	80
Figure Appendix A. 3: The simulate model in GAT system. ....	81
Figure Appendix B. 1: Composition of MGAD system (1) inner electrode (power cathode) (2) outer anodic electrode (ground) (3) wire attached to inner electrode (4) magnet (5) the arc motion between two electrodes [S.P. Gangoli, <i>et al.</i> , 2010].....	82
Figure Appendix B. 3: The simulate model in MGAD system. Diameter of injection is 2mm; diameter of outlet is 4mm; diameter and length of model is 30mm and 100mm, respectively; and Gap between electrodes is 2mm; .....	83
Figure Appendix B. 3: The simulation of MGAD reactor. Flow velocity of z axial direction at the plasma region. ....	84
Figure Appendix B. 1: The interior structure of reduction furnace.....	85
Figure Appendix B. 2: The appearance constructure of reduction furnace. ....	86



Figure Appendix B. 3: 10 wt %  $\text{Ni}_{0.35}\text{Mg}_{2.65}\text{FeO}_{4.5}/\text{Al}_2\text{O}_3$  after hydrogen reduction at the hydrogen flow rates of 50-30 sccm and 5-0.5 hr. .... 87



## Nomenclature

P Input Power

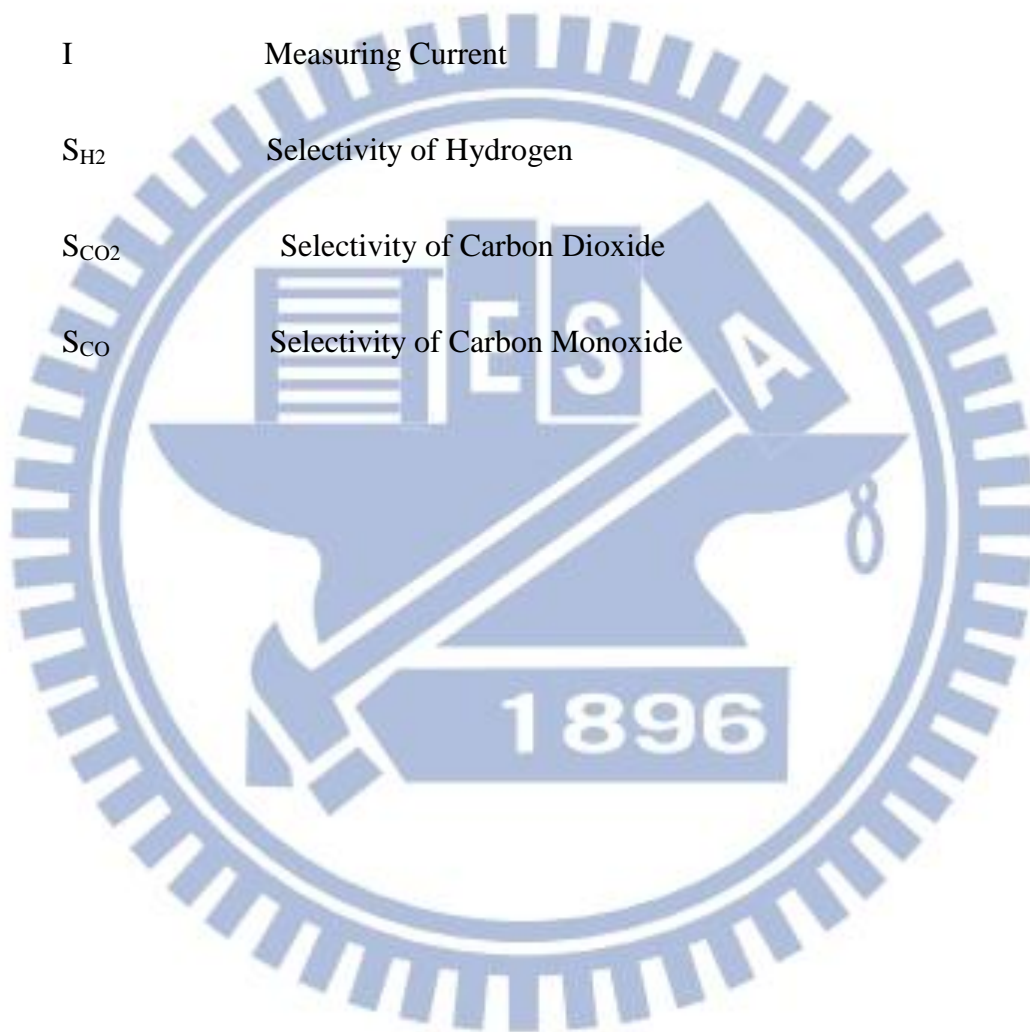
V Measuring Voltage

I Measuring Current

$S_{H_2}$  Selectivity of Hydrogen

$S_{CO_2}$  Selectivity of Carbon Dioxide

$S_{CO}$  Selectivity of Carbon Monoxide



# Chapter 1

## Introduction

### 1.1 Background and Motivation

#### *1.1.1 Hydrogen Energy Production*

In recent years, environmental pollution caused by burning fossil fuels and the depletion of fossil fuels have become serious problems that threaten the future of human civilization. Therefore, there is an urgent need to develop clean energy alternatives. Hydrogen energy possesses the highest energy content per unit weight (, i.e. 120.7 kJ/g) and is considered to be one of the most environmentally friendly energy carriers. Hydrogen can be used either directly, in a direct hydrogen combustion engine [C. M. White, 2006; J. W. Heffel, 2003; S. O. Aknsul, 2004], or in other chemical processing units, such as high-temperature solid oxide fuel cells (SOFC) [S. Park, 2000; De Seungdo, 2000; F. Zhao, 2005] and low-temperature proton exchange membrane fuel cells (PEMFC) [A. C. Dupuis, 2011; V. Mehta, 2003; J. Kim, 1995]. In the SOFC system, CO can also be used as a fuel because the system is operated at a high temperature (700-900 °C), which can easily break the strong carbon-oxygen bond. Thus, efficient production of hydrogen and CO is one of the key technologies in green energy developments such as the SOFC system.

High-temperature Solid Oxide Fuel cell (SOFC) has become a potential alternative to hydrocarbon fuel based electricity source, especially for decentralized power system, mainly due to its high thermal efficiency as compared to traditional combustion engines. In addition, carbon monoxide (CO) is a reactive gas in SOFC because of high temperature and comparably lower bonding energy of CO, while it is considered a very poisonous species for low-temperature proton exchange membrane FC (PEM-FC). Ethanol (heating value of 28.865 (kJ/kg)) is a green energy which can be produced unlimitedly from corns easily at low cost. Thus, the Center for Green Energy Technology (CGET) of NCTU has started to devote to developing an integrated SOFC system using ethanol as the fuel since 2008 (see [Figure 1.1](#) for the typical test configuration).

Ethanol represents one kind of “carbon-neutral” species since it could be produced from plants which convert sunlight and carbon dioxide through photo-synthesis reaction, and releases equal amount of carbon dioxide back to the atmosphere in the later reactive processes which generate energy. Thus, by using ethanol as the fuel source, the net amount of CO<sub>2</sub> in atmosphere remains the same and does not impact deteriorating global warming [[G. A. Deluga, 2004](#)]. This leads to the idea of using ethanol as the source in producing hydrogen, as is presented in this paper.

There are many methods of hydrogen production by reforming ethanol. They include plasma, catalyst and plasma assisted catalyst (PAC). By using plasma alone, the gliding



arc is found to be the most efficient one for hydrogen production [G. Petitpasa, 2007]. In general, the catalyst has a better efficiency of hydrogen production than the plasma alone. Application of plasma technologies on reforming of hydrocarbon fuels to generate H<sub>2</sub> has gradually attracted attention recently because of the following advantages of plasma. These include fast ignition, the compatibility for a broad range of hydrocarbons, and the high energetic density. However, by using plasma for reforming, H<sub>2</sub> selectivity is generally lower than that by using traditional catalytic reforming process [Barbara Pietruszka, 2004]. But by combining plasma and catalyst, one can possibly boost the hydrogen production [Nongnuch Rueangjitt, 2011; Yu Chao, 2008].

### ***1.1.2 Overview of Reforming Technologies***

Hydrogen production from ethanol steam reforming which is an endothermic reaction. It requires much heat to maintain the system temperature for thermal equilibrium. Thus, traditional method to produce hydrogen needs power to generate heat and needs space to provide heat generator to process endothermic steam reforming. Moreover, the reaction from ethanol to hydrogen needs catalyst to assist reaction pathways perform. Followed are introduction to traditional reforming technologies. There are many reaction pathways which include a number of dehydrogenation and dehydration path [Vizcaino *et al.*, 2007] in process, as shown in figure 1.2.

On one hand, the traditional method derived acetaldehyde from dehydrogenation of ethanol such as (2), and then methane and carbon monoxide will be produced from decarboxylation (3). Finally, it will produce hydrogen and carbon monoxide from methane steam reforming reaction.



On the other hand, ethylene will be produced from ethanol dehydration reaction (5), followed by dehydrogenation reaction (6) may poisoning in carbon accumulated which caused by loss of active. As mentioned above, ethanol steam reforming should avoid it [Vizcaino *et al.*, 2007].



In order to increase production of hydrogen, WGS (water gas shift) often use currently, as shown as (8). Thus, catalyst plays an important role in ethanol steam reforming. The catalyst can be divided into noble metal and non-noble metal, related presentations are as follows:

## 1. Noble metal catalyst

The advantage of noble metal catalyst is highly active, such as Ruthenium (Ru), Rhodium (Rh), Palladium (Pd) and Platinum (Pt). **Table 1.1** shows properties of ethanol steam reforming with different noble metal catalysts.

## 2. Non-noble metal catalyst

Some non-noble metals can also be used as hydrogen reforming catalyst which include nickel (Ni), copper (Cu), and zinc (Zn) and cobalt (Co). **Table 1.2** shows detailed performers of using different non-noble metal catalysts in ethanol steam reforming. In **Table 1.2**, the result of using nickel assist reforming can be viewed as the most effective among others; the ethanol in the reforming process easily breaks the carbon bond and produce hydrogen. Furthermore, nickel is not only the most effective catalyst but also the easiest and cheapest to prepare among others which is the reason that nickel is the most common catalyst of ethanol steam reforming.

In comprehensive surveys tender that noble catalyst (Rh) with high efficiency and non-noble catalyst ( $\text{Ni}_{0.35}\text{Mg}_{2.65}\text{FeO}_{0.45}$ ) with low-priced respectively is used to hydrogen production using ethanol as reforming fuels.

Ethanol fuel is first steamed and then flows through a catalytic reformer, which is made of rare metal oxide consisting of Ce or Ir. Although tests at the CGET of NCTU and previous studies in the literature showed very promising hydrogen conversion efficiency

(>100%, excluding the hydrogen coming from water vapor), it suffers some potential disadvantages, which include: 1) very high cost with noble catalyst (Rh) because of the rarity, and 2) lower efficiency with non-noble catalyst ( $\text{Ni}_{0.35}\text{Mg}_{2.65}\text{FeO}_{0.45}$ ) 3) short durability of the catalyst. These factors may eventually preclude the ethanol SOFC system from real applications. Thus, how to resolve the above major drawbacks of the catalytic reformer or find an alternative reformer has played an important role among one of the top priorities of the teams. In this study, we choose to find an alternative reformer, plasma or plasma assisted catalyst reformer, which is discussed later.

### ***1.1.3 Plasma Reforming Technologies***

Plasma is an ionized gas, which is generated by lots of reactor including corona, spark, glow, gliding arc discharge (GA), microwave discharge, and dielectric barrier discharge (DBD). The reforming process of hydrogen production by plasma technologies has been researched with interest for applications because plasma has following characteristics: fast ignition, the compatibility for a broad range of hydrocarbons, the high energetic density.

Plasma state is usually classified as the high temperature (or thermal) plasma and the cold (or non-thermal or non-equilibrium) plasma depending on energy level, temperature and electronic density. The most challenge to use plasma reforming process of hydrogen production is energetic efficiency. In the thermal plasma, electrons and other



species are thermal equilibrium thus the temperature can reach 10,000-100,000K, causing the reaction in thermal plasma to lack of chemical reaction selectivity. These two characters result in very little control over chemical processes inside plasma. Non-thermal plasmas are non-equilibrium in gas temperature and electron temperature and have low power requirements and are capable of inducing physical and chemical reactions within gases at relatively low temperatures. Combining these characters, non-thermal plasma has been applied for fuel gas treatment and has been considered very promising for organic synthesis. A review paper [G. Petipas, *et al.*, 2007], which has been published, shows that the yield of thermal plasma-assisted reformers is lower than non-thermal (figure 1.3). In this paper, it refers to various types of non-thermal plasma reforming technologies, which are presented in Figure 1.3 and point out the most efficient plasma sources are gliding arc (GA) by A. Fridman [A. Fridman, *et al.*, 2002]. Furthermore, in our group, we have set up a gliding arc reforming system and investigation on the gliding arc (GA) has been imperative to act. Therefore, this study focuses on gliding arc plasma for hydrogen production.

However, the H<sub>2</sub> selectivity of reforming with plasma is generally lower than with the traditional catalytic reforming process even though using non-thermal plasma-assisted reforming [B. Pietruzak, *et al.*, 2004]. Recently, a new technology has been developed, plasma-assisted catalyst (PAC), which is constructed by integrating plasma and thermal

catalysis. The PAC can be applied in hydrocarbon reforming for hydrogen production and gaseous pollutant removal. For the former application has been published in one review paper [M.B. Chang, *et al.*, 2008]. For the latter application has been published in two review papers [H.H. Ki, *et al.*, 2004; J.V. Durme, *et al.*, 2008].

For the environmental improvement, hydrogen reforming technologies are very important. Furthermore, using PAC to reform ethanol can combine the reforming advantages of using plasma-alone and using catalyst-alone, in other words PAC reforming has such advantages: rapid startup, fast response time, and fuel flexibility. Therefore, we expect PAC with gliding arc could increase the durability of the catalyst, reforming performance and H<sub>2</sub> selectivity, and turn into real application.

### ***1.1.5 Hydrocarbon Reforming Fuel***

Nowadays PAC reforming commonly uses methane as reforming fuel on the reason of methane can easily obtain from fossil fuels. However, human-caused global warming is one of the greatest and most urgent challenges that human need to deal with it on earth today. The main culprit is the enormous amount of the potent greenhouse gas carbon dioxide (CO<sub>2</sub>) released into the atmosphere by burning fossil fuels. So far, most of methane was made by fossil fuels (over 80%). In other words, using methane to generate hydrogen as clean fuel could still generate extra carbon dioxide. However, ethanol represents a type of “carbon-neutral” fuel because it is produced primarily from plants that

convert sunlight and carbon dioxide into glucose and water through photosynthesis and release an equal amount of carbon dioxide back to the atmosphere through the subsequent reactive processes that generate energy (Figure 1.5). Thus, when ethanol is used as a fuel source, the net amount of CO<sub>2</sub> in the atmosphere remains the same, and the process does not essentially affect global warming [L. D. Schmidt, *et al.*, 2004]. This leads to the idea of using ethanol as the source to produce hydrogen, which is the major objective of this paper.

Hydrogen is difficult to store and transport. Nevertheless, methane and ethanol can solve these problems. Therefore, they can be chosen as the hydrogen carrier for storage and transportation. In comparison of methane and ethanol, the energy storage ability for ethanol is better than methane. Besides, ethanol can exist on the earth in the form of liquid without extra procedure which is much safer and easier to store and transport than methane. On the basis of the advantages of using ethanol as reforming fuel, we shall emphasize on ethanol reforming.

### ***1.1.6 Literature Survey***

Since we are interested in developing a PAC system to reform ethanol, all the following literature surveys are restricted along this line. Table 1.3 and Table 1.4 summarize several important features of intermediate plasma and PAC reforming,

respectively, about experimental parameters and efficiency. Several discussions later are based on the contents of this table.

From literature surveys, plasma power input could be divided into AC power supply [Y. Kusano *et al.*, 2008, Z. Bo *et al.*, 2008], DC power supply [A. Fridman *et al.*, 2005], and pulse power supply [H. Shiki *et al.*, 2008]. Table 1.5 summarizes several power input parameters for plasma reactor, and more details are presented in Table 1.3. In the plasma system, gliding arc and GAT, power input could affect plasma characters dramatically, which could also cause synergistic effects on PAC system to change reforming results. However, there has been no systematic work in seriously studying the effects of plasma power to discharge for the same gliding arc plasma discharge.

In the plasma diagnostics parts, it is generally very difficult to measure the discharge properties inside the discharged volume. Thus, most measurements were made out of the quartz region. They include gas temperature measurements using a thermocouple [Babayan *et al.*, 2001; Wang *et al.*, 2003; Li *et al.*, 2006; Zhu *et al.*, 2005], the product gas components were analysis using gas chromatograph (figure 1.6)[Y. C. Yang *et al.*, 2009; Y. N. Chun *et al.*, 2008; M. B. Chang., *et al.*, 2008], and discharge arc column motion using high speed camera [A. Fridman *et al.*, 2000; Z. Bo *et al.*, 2007].

From the previous part of survey, the experimental parameters and conditions which could affect PAC system performance have been mentioned. Moreover, in this part of



literature survey some parameters that described the performance of reforming hydrogen have been summarized in Chapter 2.2.3 (Definition of several Performance Parameters).

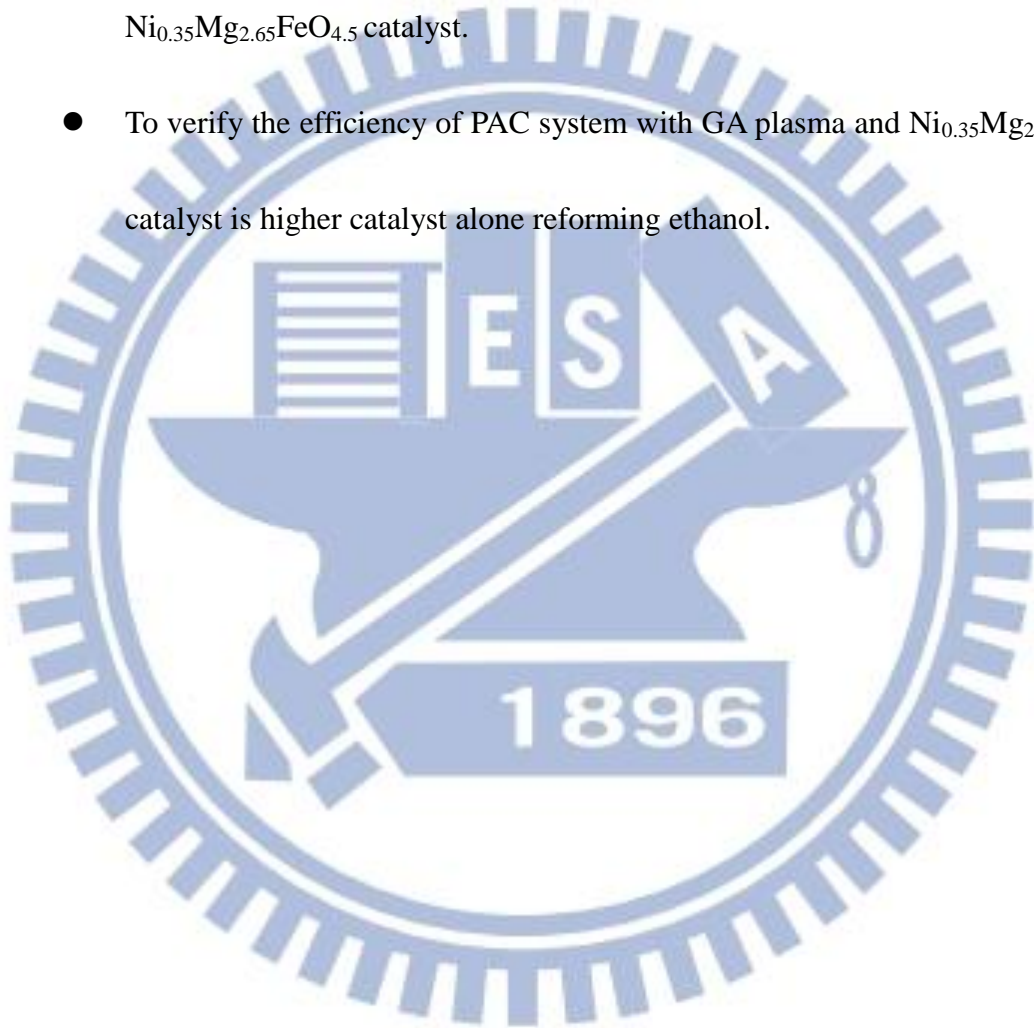
From literature survey, the conversion rate ranges is 62.6% - 87 % in [L. Bromberg *et al.*, 2006; A. Fridman *et al.*, 2002, 2005; Y. N. Chun *et al.*, 2008, 2008; M. B. Chang *et al.*, 2008; G. Petipas *et al.*, 2007]. The efficiency range from 35% - 75.81% [L. Bromberg *et al.*, 2006; A. Fridman *et al.*, 2002, 2005; Y. N. Chun *et al.*, 2008, 2008; M. B. Chang *et al.*, 2008; G. Petipas *et al.*, 2007] (Table 1.3).

## **1.2 Specific Objectives of this Thesis**

Motivated by the technical advantages and tremendous advantages of PAC reforming with gliding arc plasma with different catalyst (Rh) and ( $\text{Ni}_{0.35}\text{Mg}_{2.65}\text{FeO}_{4.5}$ ) development in this field, the objectives are summarized as followed:

- Through various C/O ratios and air flow rates, confirm the efficiency of the gliding arc (GA) reforming ethanol.
- To confirm the efficiency of the noble catalyst (Rh) reforming ethanol by adjusting various temperatures and air flow rates.
- To prove the efficiency of the PAC system with GA plasma and Rh catalyst is higher than Rh catalyst alone reforming ethanol.

- To learn how to reconstruct the non-noble catalyst ( $\text{Ni}_{0.35}\text{Mg}_{2.65}\text{FeO}_{4.5}$ ) and confirm the efficiency of the gliding arc (GA) reforming ethanol through various temperatures.
- To construct the PAC system combined the gliding arc plasma with  $\text{Ni}_{0.35}\text{Mg}_{2.65}\text{FeO}_{4.5}$  catalyst.
- To verify the efficiency of PAC system with GA plasma and  $\text{Ni}_{0.35}\text{Mg}_{2.65}\text{FeO}_{4.5}$  catalyst is higher catalyst alone reforming ethanol.



# Chapter 2

## Theoretical Method

### 2.1 Theoretical Analysis

#### *2.1.1 The Physical Phenomenon of Gliding-Arc*

The gliding arc, a discharge contains thermal and non-thermal properties, could effortlessly by two diverging knife shaped electrodes with high voltage and input power. The gliding arc starts at the smallest gap between two electrodes when the electrode field reaches breakdown conditions, for stance, an gliding arc reactor with the shortest gap about 3mm between electrodes in the atmosphere pressure, needs 10 kV to breakdown the gas, air, forming arc. And then the flow along the electrodes push the arc until the electron density could not maintain the plasma caused gliding arc is split. Finally, the next cycle starts immediately after the breakdown conditions reach. A typical gliding arc reactor has been published [A. Fridman *et al.*, 2002]. Figure 2.1 is the gliding arc reactor and the electric scheme with DC power supply and gas inlet. And, it is very important to clearly see and measure the fluctuation of current and voltage by gliding arc production in researching plasma physical phenomenon. Investigation on the electric measurement of gliding arc discharge has been published by I. Antonius [Antonius I. *et al.*, 2006].

Figure 2.2 is arc current and voltage waveform with ac power supply and shows the arc ignition with rising instantly in the current waveform of arc breakdown.

The gliding arc has been called “intermediate” plasma, having both thermal plasma and non-thermal plasma character, which offers greater energy density to perform hydrogen reforming with chemical selectivity.

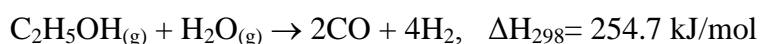
### 2.1.2 Chemical Reaction Paths of Ethanol Reforming

Nowadays, hydrogen production in the industrial procedure is “steam reforming” which is widely used all over the world, however the main drawback of this procedure is that it needs an external heat source to support reforming reaction. Furthermore, there was another hydrogen procedure, partial oxidation had been developed.

In partial oxidation reaction, ethanol reacting with insufficient oxygen generates a slightly endothermic reaction to reform ethanol into hydrogen. However, using this method lowers the performance and brings soot left caused poison of catalyst [A. Fridman *et al.*, 2004].

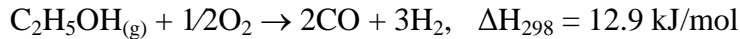
For the sake of solving these problems, combine steam reforming, water gas shift reaction and partial oxidation. Ethanol can be reformed in an “auto-thermal” [J.H. Wang *et al.*, 2009] process kept both advantages. The chemical reaction showed as followed:

Steam Reforming:

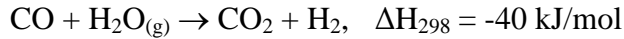




Partial Oxidation:



Water gas shift (WGS):



Auto-thermal Reforming:



### ***2.1.3 Definition of Several Performance Parameters***

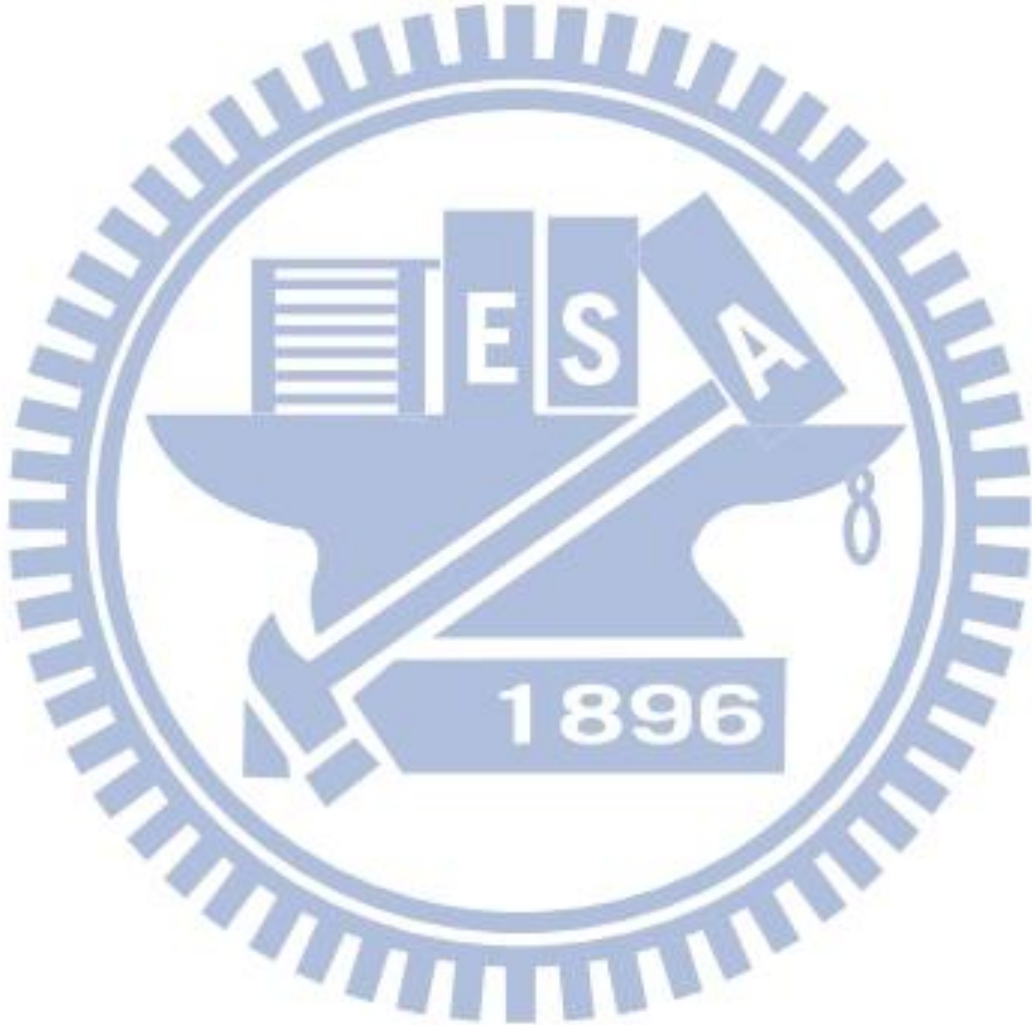
Conversion rate and selectivity are three important factors to represent the reforming performance. Each of them represents different meanings about reforming product gas composition and formula to calculate the parameter is listed below. The fuel conversion rate means how much percentage of fuel that were injected into the PAC system have been reformed into other kinds of product; the hydrogen selectivity means how much percentage of hydrogen were formed among all the formed product that contains H atoms. (Similarly, CO selectivity and CO<sub>2</sub> selectivity represent same idea, if there were other formed product gases); the reformer thermal efficiency represents the proportion of the lower heating value (LHV) of formed hydrogen to the input energy, that is the summation of the electrical energy of the plasma and the LHV of the hydrocarbon injected [G. Petitpas *et al.*, 2009].

The methods of data analysis are shown as following Equations.

$$\text{Selectivity (H}_2\text{)} = \frac{\text{Amount of H atoms in the formed H}_2}{\text{Amount of H atoms in the formed product}} \quad (9)$$

$$\text{Fuel Conversion Rate (\%)} = \frac{[\text{Input fuel}] - [\text{Output fuel}]}{[\text{Input fuel}]} \quad (10)$$

$$\text{Efficiency} = \frac{(\text{H}_2 + \text{CO})_{\text{produced}} \times \text{LHV}(\text{H}_2)}{\text{Input plasma energy} + \text{fuel injected} \times \text{LHV}(\text{Fuel})} \quad (11)$$



# Chapter 3

## Experimental Methods

### 3.1 Overview of Experimental Setup

**Fig 3.1** shows a schematic diagram of the experimental arrangement. It consists of a fuel source zone (ethanol/water mixture and air), a preheating zone, a gliding-arc plasma zone, and a catalyst reactor. The steaming fuel flow was first preheated by a heating furnace. Then, the flow passed through the plasma reactor and finally the catalyst reactor, with the furnace temperature maintained at 380 °C. After reforming in the catalyst bed, the gases were sampled using gas chromatography (GC; YL 6100GC, Young Lin Instrument Co., Ltd **Figure 3.2**) with a pulsed discharge helium ionization mode detector (PDHID). In transporting the gases from the furnace to the gas chromatography equipment, a 2-m heated tube was used to prevent the gases from condensing on the tube wall. The sampled gases were analyzed with a mass-balance error of less than 10%. The experimental configurations and operating conditions of each subsystem are described in detail in the following next sections.

## **3.2 Experimental Facilities**

In this section, the contents particularly give an account for experimental facilities, including plasma reactor which is divided into gliding-arc and magnetic gliding-arc discharge; ac power supply; fuel feeding; and catalyst preparation.

### ***3.2.1 Plasma Reactor***

**Figure 3.3** shows the sketch of an in-house designed gliding arc reactor. This reactor consists of two 30 mm long, 7 mm wide and 2 mm thick knife-shaped electrodes fixed on a Peak bed plate, which can sustain at temperature up to 315 °C. The electrodes of gliding arc are made of stainless steel. A quartz tube with inner diameter 22 mm and 55 mm long is inserted and well-sealed with the Peak bed plate. The ethanol steam flows from the bottom and passes through the reactor. By applying the voltages across the electrodes, arc starts at the location of smallest gaps between the two electrodes. Arc is carried downstream by the air, and then becomes weaker and weaker because of smaller electric field (larger gap) and finally extinguishes. The next cycle of arc starts immediately after the breakdown condition reached at the throat.

### ***3.2.2 AC Power Supply and Pulse Generator***

The power supply (PVM500 plasma driver, Information Unlimited Inc. **Figure 3.4**) supplies the gliding arc plasma with high voltage and frequency. It has independent



voltage control ranges from zero to maximum 20 kV peak-to-peak. And frequency ranges from 20-70 kHz. Though, this power supply is relatively unstable compare to others, its price was low (\$449.95). In the next chapter, the influence of different output power magnitude on electrical character and reforming efficiency was studied in detail.

### ***3.2.3 Fuel Feeding and Heating System***

Ethanol and water, supplied by a liquid pump (930d-1428, Young Lin Instrument CO., Ltd., 0.0005-1.0 SLM, **Figure 3.5**), were mixed with dry air from a compressor controlled by a mass flow controller (Multi-gas MFC, MC-100SCCM-D, Alicat Scientific Inc., max. 100 sccm, **Figure 3.5**). The gases were injected into the preheating zone (to raise the temperature) through an oil injector that was taken from a car engine and controlled by a solenoid valve (Fuel Injection, Mitsubishi Eclipse, **figure 3.6**). The solenoid valve was operated with a voltage of 12 volts, and the duty cycle could be adjusted to control the valve opening time. This injector was adjusted to maximize the vaporization of water and ethanol droplets by varying the duty cycle of the input driving voltage. Through this setup, one can control experimental parameters such as, the C/O mole ratio, air flow rate, and ethanol/water mole ratio. C/O (mole) ratio represents the ratio of the moles of C in the inflowing ethanol to the moles of O in the inflowing mixture that consisted of ethanol, water and air. High-purity ethanol (99%) was used as the fuel and was mixed together uniformly using an ultrasonic wave mixer before injection by the liquid pump.

The heating system consists of two heating furnaces that were heated at specific temperatures to control the gasification and catalyst reaction (You & Me Inc., [Figure 3.7](#)).

### **3.2.4 Catalyst Preparation**

Thanks to professor Lee, Department of Applied Chemistry, NCTU for sharing the chemicals and skills. All the catalyst setup procedures are learned from professor Lee's laboratory.

#### **3.2.4.1 Rh/CeO<sub>2</sub>/Al<sub>2</sub>O<sub>3</sub>**

The reforming catalyst beads were prepared using 5% Rh/CeO<sub>2</sub>/Al<sub>2</sub>O<sub>3</sub>. Initially, 1 g of porous Al<sub>2</sub>O<sub>3</sub> beads to be used as carriers were ground to small pieces, with a volume in the range of 1.00-1.41 mm<sup>3</sup>. These were subsequently mixed with an ethanol solution containing 0.125 g of dissolved Ce(NO<sub>3</sub>)<sub>3</sub> and heated to 50 °C to evaporate the ethanol. Thereafter, the Al<sub>2</sub>O<sub>3</sub> carriers loaded with Ce(NO<sub>3</sub>)<sub>3</sub> were sintered at 300 °C for 5 hours. In addition, 0.01 g of RhCl<sub>3</sub> in an ethanol solution was prepared and mixed with 10 % Ce-Al<sub>2</sub>O<sub>3</sub> after sintering. Following the same procedure for evaporating the ethanol, the 10% Ce-Al<sub>2</sub>O<sub>3</sub> loaded with 5% RhCl<sub>3</sub> was placed into the furnace at 600 °C and 200 sccm of hydrogen was pumped for 6 hours for the reduction. In addition, 1 g of porous Al<sub>2</sub>O<sub>3</sub> loaded with 5% Rh/CeO<sub>2</sub> could be produced using the above procedure. The procedure is presented in [Figure 3.8](#).

### 3.2.4.2 $Ni_{0.35}Mg_{2.65}FeO_{4.5}/Al_2O_3$

The preparation for Ni/Mg/Al catalyst is done by coprecipitation method. First, the mass of  $Ni(NO_3)_3$ ,  $Mg(NO_3)_2$ , and  $Fe(NO_3)_3$ , which respectively are 0.2139 g, 1.4485 g, and 0.8484 g, is changed the PH from acidity to 10.5 by titration using the alkaline liquid mixed the NaOH of 6 g with the  $Na_2CO_3$  0.99375 g. And then dry the product made by above the elements to form the important admixture,  $Ni_{0.35}Mg_{2.65}FeO_{4.5}$ . To pestle the admixture with 95 Vol.% ethanol and let the admixture can be easily coat in the carrier,  $Al_2O_3$ , in the specific ratio of mass weight of  $Ni_{0.35}Mg_{2.65}FeO_{4.5}/Al_2O_3$  is 0.1 . Finally, the reduction furnace, which specially designed to solve the hydrogen waste by traditional reduction method, is used to reduce the 10 wt%  $Ni_{0.35}Mg_{2.65}FeO_{4.5}/Al_2O_3$  at 500 °C furnace keeping 30 min (figure 3.9). The figure 3.9 is simple flowchart for preparing this catalyst.

## **3.3 Experimental Instrumentation**

In the plasma and plasma assisted catalyst reforming, the power supply (PVM500 plasma driver) system which has the voltage control ranging from zero to maximum 20 kV peak-to-peak at a frequency of 20 kHz. Meanwhile, we use the High Voltage Probe (Fig 3.10) to measure plasma voltage and Rogowski coil (Fig 3.11) to measure the current respectively. The measured voltage and current are recorded using an oscilloscope (Tektronix TDS1012B Fig 3.11). In the following, several key components of the plasma

assisted catalytic system are introduced in turn. After reforming process, the productions are measured and sampled by gas chromatography (Figure 3.2).

## **3.4 Experimental Procedures**

### ***3.4.1 Catalytic Reforming***

In catalytic reforming, the steaming fuel was first preheated by a heating furnace. Then, the flow, including air, ethanol, and DI water, passed through catalysis bed. Finally, the gases were sampled using gas chromatography.

### ***3.4.2 Plasma Reforming***

In plasma reforming, the ethanol mixed water was injected by a liquid pump and preheated by a heating furnace respectively. After the fuel consisted of air and ethanol mixed water went through the plasma zone, we used the chromatography to sample the productive gases.

### ***3.4.3 Plasma Assisted Catalytic Reforming***

In Plasma Assisted Catalytic Reforming, we used the air pump and liquid pump to inject the air and ethanol mixed water respectively. Then, the fuel went through the plasma zone and finally the catalyst reactor. The productive gases from reforming were sampled by gas chromatography.



### **3.5 Test Conditions**

In this study, air flow rates were controlled and maintained in the range of 0.5-2.0 slm, the inflow C/O ratio was fixed at 0.7 unless otherwise specified, and the molar ratio of ethanol to Deionized water (DI) water was kept at 1:3 (the flow rate of ethanol/DI water mixture was 0.57-1.7 sccm). Gasification temperature in the preheat zone and the furnace temperature for the catalyst bed were kept at 160 °C and 230 °C, respectively. The power input for the gliding-arc device was fixed as 223 W throughout the study.

The test conditions for the gliding arc plasma, catalyst (Rh/CeO<sub>2</sub>/Al<sub>2</sub>O<sub>3</sub>), and PAC with gliding arc reforming are summarized in [table 3.1](#). And the test conditions for catalyst (Ni<sub>0.35</sub>Mg<sub>2.65</sub>FeO<sub>4.5</sub>) are summarized in [table 3.2](#).

# Chapter 4

## Characterization of Gliding Arc Plasma

### 4.1 Visualization

The **figure 4.1** shows the typical images of the gliding arc discharge using air flow rate in 1.5 SLM and 200 w with 20 kHz, supplied by AC power. And the **figure 4.2** shows the comparison between the gliding-arc plasma injecting ethanol mixed water or not. Obviously, the colors and length of blazes are distinct from the the addition of fuel at a C/O ratio of 0.7. The above images was captured by High Speed Camera with the maximum frame rate 1200 fps.

### 4.2 Elecreical Properties

**Figure 4.3** shows the typical measured input vlotage (20kHz) and plasma current waveforms under the conditions, including fuel at a C/O ratio of 0.7, gas temperature 160 °C, and air flow rate in 1.5 SLM. Through the equation of integration (12), the obtainable plasma absorption power is 223 W.

$$\text{Absorption Power} = \frac{\sum (I_n \times V_n)}{T_{\text{measured time}}} \quad (12)$$

# Chapter 5

## Results and Discussion

### 5.1 Reforming with Gliding Arc Plasma

#### *5.1.1 Effect of C/O ratio*

**Figure 5.1** shows the variation in the conversion rate, H<sub>2</sub> selectivity and CO<sub>2</sub> selectivity with changes to the C/O ratio at an air flow rate of 1.5 SLM. When the C/O ratio is 0.3, the conversion rate is at its highest; however, the H<sub>2</sub> selectivity is at its lowest. When the C/O ratio becomes 0.7, the H<sub>2</sub> selectivity reaches its maximum (43%) and the conversion rate decreases to 35%, which represents the best reforming performance when using plasma alone. Fortunately, this optimized condition (C/O ratio of 0.7) also coincides with optimal Rh catalyst reforming, which was used in the current study [Wang Q *et al.*, 2009]. For this reason, all the PAC experiments were conducted at a C/O ratio of 0.7.

#### *5.1.2 Effect of Gas Flow Rate*

**Figure 5.2** shows the selectivity of hydrogen and carbon dioxide and the fuel conversion rate as functions of the air flow rate. The fuel conversion rate is generally less than 40% and less than 30% at the maximal air flow rate (2.0 SLM). The dramatic

decrease in the fuel conversion rate at 2.0 SLM can be attributed to the short residence time in the plasma reactor because of the high gas flow rate. In addition, the hydrogen selectivity and the fuel conversion rate both peak at an air flow rate of 1.5 SLM [Rueangjitt N. *et al.*, 2011, Chernyak V.Y. *et al.*, 2008].

Figure 5.3 shows the H-selectivity of methane, water and hydrogen, each as a function of the air flow rate. There is nearly no methane produced when the air flow rate is larger than 0.5 SLM because of the shorter residence time of steaming ethanol in the plasma reactor. The main products that contain H atoms are hydrogen and water vapor. The highest H-selectivity of hydrogen is 43% and the lowest H-selectivity of water vapor is 57% at an air flow rate of 1.5 SLM.

Figure 5.4 shows the C-selectivity of methane, carbon monoxide and carbon dioxide, each as a function of the air flow rate. The highest C-selectivity of carbon monoxide is 75%, and the C-selectivity is 25% at an air flow rate of 1.0 SLM. This shows that a large amount of carbon monoxide can be produced at all of the air flow rates considered in this study.

## **5.2 Catalyst Reforming**

In this section, investigation on conversion rates, hydrogen and carbon dioxide selectivity of catalyst reforming is divided into two parts to discuss the results. First part is the catalyst reforming with Rh noble catalyst to confirm the selectivity and conversion



at different air flow rates (0.5-2.0 SLM). And the second part is the catalyst reforming with Ni<sub>0.35</sub>Mg<sub>2.65</sub>FeO<sub>4.5</sub>/Al<sub>2</sub>O<sub>3</sub> to confirm the selectivity and conversion at different temperatures (200-400 °C).

### 5.2.1 Rh

Figure 5.5 shows the conversion rates, hydrogen selectivity and carbon dioxide selectivity at different air flow rates with the C/O ratio maintained at 0.7. At an air flow rate of 1.0 SLM, Hydrogen selectivity ( $S_{H_2}$ ) is found to be more than 100 % and the conversion rate is nearly 100% (98%). However, when the flow rate increases to 1.5 SLM or 2 SLM, the reforming efficiency becomes worse (~70%). This can be attributed to the shorter residence time during which the catalyst cannot thoroughly react with the gases. However, at an air flow rate of 0.5 SLM, even though the residence time is the longest, the catalyst reforming performance is not better than at air flow rates of 1.0 or 1.5 SLM. This results from the catalyst reforming becoming favorable to the complete oxidation reaction ( $C_2H_5OH + 3O_2 \rightarrow 2CO_2 + 3H_2O$ ) [Wang Q *et al.*, 2009], which prevents the production of hydrogen. The above observations show that higher reforming efficiencies can be obtained only at specific air flow rates using the catalyst bed with 5% Rh/CeO<sub>2</sub>/Al<sub>2</sub>O<sub>3</sub>, which necessitates a remedial approach for extending the applicability of ethanol reforming, such as plasma-assisted catalyst reforming.

### 5.2.2 Ni<sub>0.35</sub>Mg<sub>2.65</sub>FeO<sub>4.5</sub>/Al<sub>2</sub>O<sub>3</sub>

Figure 5.6 shows the conversion rate, hydrogen selectivity and carbon dioxide selectivity at different temperatures. Obviously, the hydrogen selectivity and ethanol conversion rates of Ni<sub>0.35</sub>Mg<sub>2.65</sub>FeO<sub>4.5</sub>/Al<sub>2</sub>O<sub>3</sub> catalyst (non-noble) are much lower than the Rh catalyst (noble). In the section 1.1.2 has introduced that the efficiency of noble catalyst almost higher than non-noble catalyst. Therefore, it is no surprise to the results.

Figure 5.6 also shows the hydrogen and selectivity dropped down with adjusting decreasingly catalyst temperatures. However, the catalyst temperatures stand for the energy provided. Furthermore, the effect of catalyst temperature has been presented at the IJHE paper [M. Li and *et al.*, 2010]. The catalyst is much more inefficient at water-gas-shift chemical reaction.

### **5.3 Plasma Assisted Catalyst (PAC) Reforming**

In this section, investigation on hydrogen and carbon dioxide selectivity and conversion rates of PAC reforming is divided into two parts to discuss the results. Owing to compare the catalyst reforming with PAC reforming, the test parameters of catalyst needed to be the same. Therefore, first part is the PAC reforming with Rh noble catalyst and gliding arc plasma to confirm the selectivity and conversion rates at different air flow rates (0.5-2.0 SLM). And the second part is the PAC reforming with

$\text{Ni}_{0.35}\text{Mg}_{2.65}\text{FeO}_{4.5}/\text{Al}_2\text{O}_3$  and gliding arc plasma to confirm phenomenon at the temperatures (400 °C) which arise the highest selectivity and conversion rate in catalyst reforming.

### 5.3.1 PAC reforming with Rh catalyst

Figure 5.7 shows the conversion rates, hydrogen selectivity and carbon dioxide selectivity at different air flow rates for different cases of PAC. At an air flow rate of 0.5 SLM, the hydrogen selectivity and the conversion rate of PAC are 72% and 98%, respectively, which are lower than those for the pure catalyst reforming. This could be attributed to the longer residence time in the plasma reactor at the lowest air flow rate, which produces smaller molecules such as  $\text{C}_2\text{H}_4$  and  $\text{C}_2\text{H}_6$  (see Table 5.1) that are measured by gas chromatography, resulting in smaller hydrogen selectivity.

Notably, Figure 5.7 also shows that the fuel conversion rate and hydrogen selectivity for the PAC case are high, at 100% and 111.2%, respectively, at an air flow rate of 1.5 SLM. Without the addition of plasma, the hydrogen selectivity is very low (~70%) at this air flow rate because of the shorter residence time, as explained earlier and also in the literature [Barbara Pietruszka, 2004, Yu Chao, 2008]. From Figure 5.2, we have learned that the hydrogen selectivity the highest with plasma alone at this air flow rate. Furthermore, Figure 5.3 also demonstrates that plasma reforming produces appreciable

CO, which is able to assist the catalyst reforming through the water-gas-shift reaction ( $\text{CO} + \text{H}_2\text{O} \rightarrow \text{CO}_2 + \text{H}_2$ ), which was also reported in [Wang Q *et al.*, 2009].

### 5.3.2 PAC reforming with $\text{Ni}_{0.35}\text{Mg}_{2.65}\text{FeO}_{4.5}$ Catalyst

If the hydrogen selectivity and conversion rates of non-noble catalyst could be raised to close the noble catalyst, the economic benefit would be elevatory causing the reforming cost dropped down rapidly. However, the results in [figure 5.8](#) and [figure 5.9](#) show that, even though the PAC system with  $\text{Ni}_{0.35}\text{Mg}_{2.65}\text{FeO}_{4.5}$  catalyst could improve the hydrogen selectivity and conversion rate, the outcome is much worse than with the Rh catalyst. The reason perhaps is that this catalyst has the inefficiently water-gas-shift chemical reaction with gliding arc generated much  $\text{H}_2\text{O}$  ([figure 5.3](#)). Therefore, The suggestion, decreased the ratio of ethanol mixed water and inject lesser DI water to PAC reforming with gliding arc and  $\text{Ni}_{0.35}\text{Mg}_{2.65}\text{FeO}_{4.5}$  catalyst, should be published for the future work.



# Chapter 6

## Conclusion and Future Work

### 6.1 Conclusion

In this study, ethanol steam flow is reformed using a gliding-arc plasma-assisted catalytic system with air flow rates in the range of 0.5-2.0 SLM. The results show that, with the catalyst alone, a 100% conversion rate and a maximum of 115% hydrogen selectivity were obtained at a C/O ratio of 0.7 with an air flow rate of 1.0 SLM. However, the hydrogen selectivity decreases rapidly to 95%, 70% and 68%, respectively, at air flow rates of 0.5, 1.5 and 2.0 SLM. The former can be attributed to the longer residence time in the catalytic bed, causing a higher temperature that favors a complete oxidation reaction ( $C_2H_5OH + 3O_2 \rightarrow 2CO_2 + 3H_2O$ ). The latter two cases can be attributed to the shorter residence time, which is not enough time for a complete catalytic reaction to occur. With the addition of the gliding-arc plasma, the hydrogen selectivity reaches 113% and 111.2% at air flow rates of 1.0 and 1.5 SLM, respectively. This shows that, with the use of the gliding-arc plasma prior to the catalyst, a very high hydrogen selectivity (>110%) can be obtained at air flow rates of 1.0 or 1.5 SLM with the current experimental setup. However, at an air flow rate of 2.0 SLM, the hydrogen selectivity of PAC drops down to less than

70% and is nearly the same as that for catalyst reforming. This is attributed to the shorter residence time in the plasma reactor, resulting in no assistance from the gliding arc. Thus, we can conclude that a very high reforming efficiency can be obtained at air flow rates less than 2.0 SLM using the PAC system developed in the current study. In this study, we have learned that the residence time within the plasma reactor and the catalyst reactor is a key parameter that needs to be controlled properly to obtain good hydrogen selectivity for ethanol steam reforming. For better control, an improved system adapted from a tornado gliding arc (TGA) [Kalra C.S., Fridman A., 2003, 2005] is currently being developed in our group and will be reported in the near future.

In the  $\text{Ni}_{0.35}\text{Mg}_{2.65}\text{FeO}_{4.5}$  Catalyst Reforming, the highest hydrogen selectivity (~55%) and conversion rate are close to 100% at temperature 400 °C and drop down rapidly with decreasing the temperature. However, the PAC with  $\text{Ni}_{0.35}\text{Mg}_{2.65}\text{FeO}_{4.5}$  Catalyst can improve the selectivity of catalyst alone reforming to 75%. Even though the selectivity could be raised, the conversion rate drops down to 73%. The reason maybe the plasma generates a lot of  $\text{H}_2\text{O}$  but the catalyst is inefficient at water-gas-shift (WGS) chemical reaction equation. Hence, to change the C/O ratio and ethanol mixed water with different from 1:3 is a possible to solve the worse WGS reaction in  $\text{Ni}_{0.35}\text{Mg}_{2.65}\text{FeO}_{4.5}$  catalyst.

## **6.2 Recommendations for Future Work**

- i. To adjust the temperatures in PAC system with Rh catalyst for much better reforming selectivity.
- ii. To change the ratio of water mixed ethanol to solve the  $\text{Ni}_{0.35}\text{Mg}_{2.65}\text{FeO}_{4.5}$  catalyst is worse in WGS reaction.
- iii. To design the MGAD for the shorter residence time of PAC with gliding at higher air flow rate. The detailed design and simulate has been done and showed in Appendix B.
- iv. To raise the catalyst reforming temperature for confirm the highest selectivity  $\text{Ni}_{0.35}\text{Mg}_{2.65}\text{FeO}_{4.5}$ .
- v. To exchange the sequence between plasma and catalyst in PAC system for investigation on the variation.
- vi. To combine the plasma with other non-noble catalyst, which has better selectivity and simultaneously is low cost.
- vii. To investigate that the effect of gaps between two electrodes in gliding arc plasma for hydrogen production.
- viii. To analyze the chemical reaction in plasma alone, catalyst alone, and PAC reforming.

## References

1. Akansul S.O., Dulger Z., Kahraman N., Nejat Veziroglu T. “Internal combustion engines fueled by natural gas—hydrogen mixtures”, International Journal of Hydrogen Energy, 29, pp. 1527-1539, 2004.
2. Barbara Pietruszka, Moritz Heintze, “Methane conversion at low temperature: the combined application of catalysis and non-equilibrium plasma,” Catalysis Today, 90, pp. 151-158, 2004
3. Batista, M.S., Santos, R.K.S., Assaf, E.M., Assaf, J.M., and Ticianelli, E.A., “High efficiency steam reforming of ethanol by cobalt-based catalysts”, Journal of Power Sources, 134, pp. 27-32, 2004.
4. Bo Z., Yan J.H., Li X.D., Chi Y., and Cen K.F. “ Scale-up analysis and development of gliding arc discharge facility for volatile organic compounds decomposition”, Journal of Hazardous Material, 155, pp. 494-501, 2004.
5. Bo Z., Yan J.H., Li X.D., Chi Y., Cheron B., Cen K.F. “The dependence of gliding arc gas discharge characteristics on reactor geometrical configuration”, Plasma Chemistry and Plasma Processing, 27, pp. 691-700, 2007.
6. Bo, Z., Yan J., Li X.D., Chi Y., Cen K. “Plasma assisted dry methane reforming using gliding arc gas discharge: Effect of feed gases proportion”, International Journal of



- Hydrogen Energy, 33, pp. 5545-5553, 2008.
7. Bromberg L., Cohn D.R., Rabinovich A., Alexeev N., Samokhin A., Hadidi K., Palaia J., N. Margarit-Bel, “Onboard Plasmatron Hydrogen Production for Improved Vehicles”, PSFC JA-06-3, 2006.
  8. Cavallaro S., Chiodo V., Freni S., Mondello N., Frusteri F. “Performance of Rh/Al<sub>2</sub>O<sub>3</sub> catalyst in the steam reforming of ethanol: H<sub>2</sub> production for MCFC”, Applied Catalysis A: General, 249, pp. 119-128, 2003.
  9. Chao Y., Huang C. T., Chang M. B., Lee H. M. “Hydrogen production via partial oxidation of methane with plasma-assisted catalysis,” International Journal of Hydrogen Energy, 33, pp 664-671, 2008.
  10. Chao Y., Huang C.T., Lee H.M., and Chang M.B. “ Hydrogen production via partial oxidation of methane with plasma-assisted catalysis”, International Journal of Hydrogen Energy,33, pp. 644-671, 2008.
  11. Chen H.L., Lee H.M., Chen S.H., Chao Y., Chang M.B. “ Review of plasma catalysis on hydrocarbon reforming for hydrogen production-Interaction, integration, and prospects”, Applied Catalysis B-Environmental, 85, pp. 1-9, 2008.
  12. Chernyak V.Y., Olszewski S.V., Yukhymenko V.V., Solomenko E.V., Prysiazhnevych I.V., Naumov V.V., Levko D.S., Shchedrin A.I., Ryabtsev A.V., Demchina V.P., Kudryavtsev V.S., Martysh E.V., Verovchuck M.A. “Plasma-Assisted Reforming of

- Ethanol in Dynamic Plasma-Liquid System: Experiments and Modeling”, IEEE Transaction On Plasma Science, pp. 36(6), 2933 – 2939, 2008.
13. Cohn D.R., Rabinovich A., Titus C.H., and Bromberg, L. International Journal of Hydrogen Energy, Elsevier, 22, pp. 715–723, 1997.
  14. Comas J., Mariño F., Laborde M., Amadeo N. “Bio-ethanol steam reforming on Ni/Al<sub>2</sub>O<sub>3</sub> catalyst”, Chemical Engineering Journal, 98, pp. 61-68, 2004.
  15. De Souza S., Visco S.J., Jongle L.C.D. “Thin-film solid oxide fuel cell with high performance at low-temperature”, Solid State Ionics, 98, pp. 57-61, 1997.
  16. Diagne C., Idriss H., and Kiennemann A. “Hydrogen production by ethanol reforming over Rh/CeO<sub>2</sub>–ZrO<sub>2</sub> catalysts”, Catalysis Communications, 3, 565-571, 2002.
  17. Dupuis A.C. “Proton exchange membranes for fuel cells operated at medium temperatures: Materials and experimental techniques”, Progress in Materials Science, 56, pp. 289-327, 2011.
  18. Erdohelyi A., Raskó J., Kecskés T., Tóth M., Dömök M., and Baán K. “Hydrogen formation in ethanol reforming on supported noble metal catalysts”, Catalysis Today, 116, 367-376, 2006.
  19. Fatsikostas, A.N., Verykios X.E. “Reaction network of steam reforming of ethanol over Ni-based catalysts”, Journal of Catalysis, 225, pp. 439-452, 2004.
  20. Fields, S., “Hydrogen for Fuel Cells: Making the Best of Biomass”, Environmental

Health Perspectives, 111, pp. A38-A41, 2003.

21. Frusteri F., Freni S., Chiodo V., Spadaro L., Di Blasi O., Bonura G., Cavallaro, S. “Steam reforming of bio-ethanol on alkali-doped Ni/MgO catalysts: hydrogen production for MC fuel cell”, Applied Catalysis A: General, 270, pp. 1-7, 2004.
22. Frusteri F., Freni S., Spadaro L., Chiodo V., Bonura G., Donato S., Cavallaro, S. “H<sub>2</sub> production for MC fuel cell by steam reforming of ethanol over MgO supported Pd, Rh, Ni and Co catalysts”, Catalysis Communications, 5, pp. 611-615, 2004.
23. G. A. Deluga, J. R. Salge, L. D. Schmidt, X. E. Verykios, 2004, “Renewable Hydrogen from Ethanol by Autothermal Reforming,” Science, 303, pp. 993-996.
24. G. Petitpas, J.D. Rollier, A. Darmon, J. Gonzalez-Aguilar, R. Metkemeijer, and L.Fulcheri, “A comparative study of non-thermal plasma assisted reforming technologies”, International Journal of Hydrogen Energy, 32, pp.2848-2867, 2007.
25. Heffel J.W. “NO<sub>x</sub> emission and performance data for a hydrogen fueled internal combustion engine at 1500 rpm using exhaust gas recirculation”, International Journal of Hydrogen Energy, 28, pp. 901-908, 2003.
26. Indarto A., Choi J. W., Lee H., Song H. K., Coowanitwong N. “Discharge characteristics of a gliding-arc plasma in chlorinated methanes diluted in atmospheric air” Plasma Device and Operations, 14, 15-26, 2006.
27. Kalra C. S., Kossitsyn M., Iskenderova K., Chirokov A., Cho Y. I., Gutsol, A., and

- Fridman, A., Electronic Proceedings of the 16th International Symposium on Plasma Chemistry, Taormina, Italy, pp.22–27, 2003.
28. Kalra C.S., Cho Y.I., Gutsol A., Fridman A., and Rufael, T.S., “Gliding arc in tornado using a reverse vortex flow”, Review of Scientific Instruments, 99, 76, 2005.
29. Kalra C.S., Cho Y.I., Gutsol A., Fridman A., and Rufael, T.S., “Non-Thermal Plasma Catalytic Conversion of Methane to Syn-Gas”, Abstracts of Papers of the American Chemical Society, 228, pp. 687, 2004.
30. Kalra C.S., Gutsol A.F., and Fridman A.A., “Gliding arc discharges as a source of intermediate plasma for methane partial oxidation”, IEEE, Transactions of Plasma Science, 33, pp. 32-4, 2005.
31. Kim J, Lee S.M., Srinivasan S. “Modeling of Proton Exchange Membrane Fuel Cell Performance with an Empirical Eq”, Journal of The Electrochem Society, 142, pp. 2670-2674, 1995.
32. Kusano Y., Teodoru S., Leipold F., Andersen T.L., Sorensen B.F. Rozlosnik N., Michelsen P.K. “Gliding arc discharge - Application for adhesion improvement of fibre reinforced polyester composites”, Surface & Coatings technology, 202, pp. 5579-5582, 2008.
33. Kuznetsova I.V., Kalashnikov N.Y., Gutsol A.F., Fridman A.A., and Kennedy L.A. “Effect of "overshooting" in the transitional regimes of the low-current gliding arc

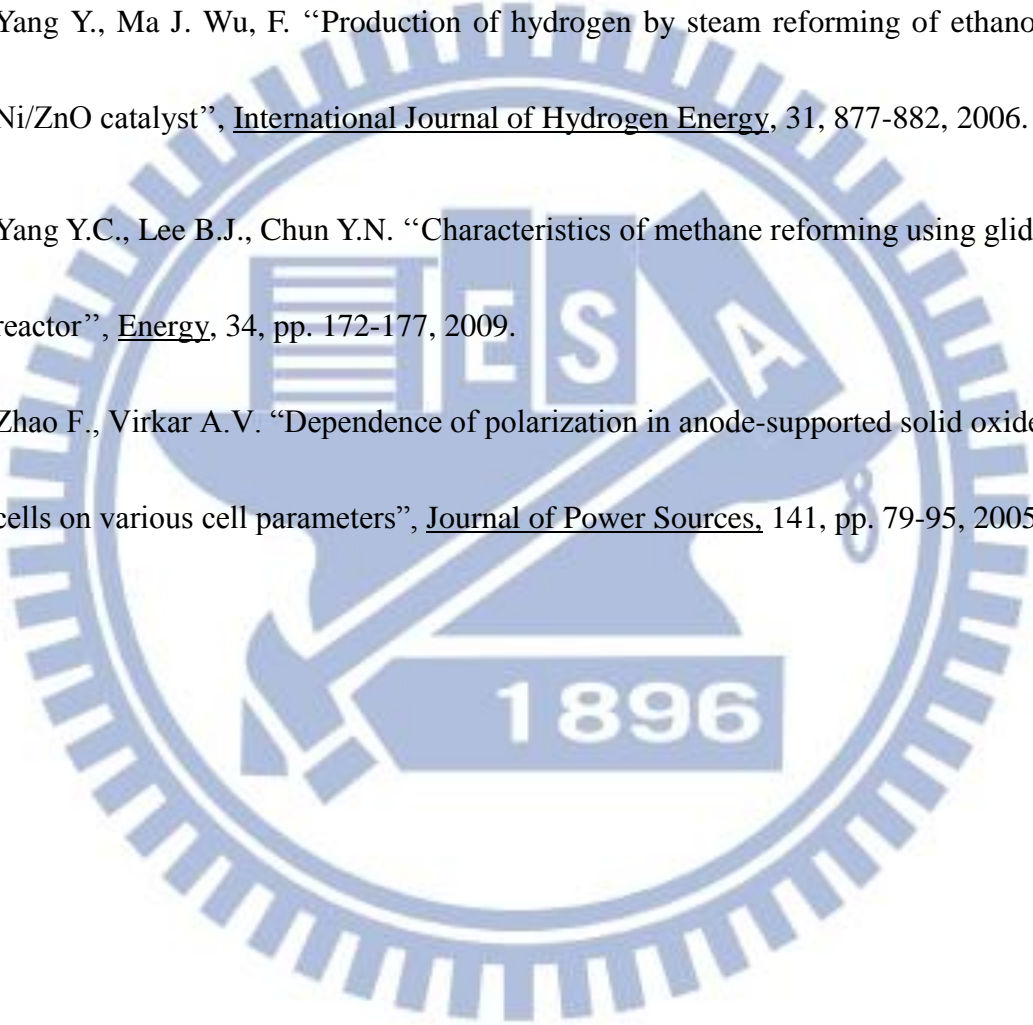


- discharge”, Journal of Applied Physics, 92, pp. 4231-4237, 2002.
34. Li M., Wang X., Li S., Wang S., Ma X. “Hydrogen production from ethanol steam reforming over nickel based catalyst derived from Ni/Mg/Al hydrotalcite-like compounds”, International Journal of Hydrogen Energy, 35, pp. 6699-6708, 2010
35. Liguras D.K., Kondarides D.I., Verykios X.E. “Production of hydrogen for fuel cells by steam reforming of ethanol over supported noble metal catalysts”, Applied Catalysis B: Environmental, 43, pp. 345-354, 2003.
36. Llorca J., Homs N., Sales J., Fierro J.L.G., Piscina P.R. “Effect of sodium addition on the performance of Co–ZnO-based catalysts for hydrogen production from bioethanol”, Journal of Catalysis, 222, pp. 470-480, 2004.
37. Llorca J., Piscina P.R., Dalmon J.A., Sales J., Homs N. “CO-free hydrogen from steam-reforming of bioethanol over ZnO-supported cobalt catalysts: Effect of the metallic precursor”, Applied Catalysis B: Environmental, 43, pp. 355-369, 2003.
38. Mehta V., Cooper J.S.. “Review and analysis of PEM fuel cell design and manufacturing”, Journal of Power Sources, 114, pp. 32-53, 2003.
39. Mutaf-Yardimci O., Saveliev A.V., Fridman A.A. and Kennedy L.A. “Thermal and non-thermal regimes of gliding arc discharge in air flow”, Journal of Applied Physics, 87, pp. 1632-1641, 2000.
40. P. J. de Wild, Verhaak M. J. F. M. “Catalytic production of hydrogen from methanol,”

Catalysis Today, 60, pp. 3-10, 2000.

41. Park Seungdo, Vohs J.M., Gorte R.J. "Direct oxidation of hydrocarbons in a solid-oxide fuel cell", Nature, 404, pp. 265-267, 2000.
42. Rueangjitt N., Sreethawong T., Chavadej S., Sekiguchi H. "Non-Oxidative Reforming of Methane in a Mini-Gliding Arc Discharge Reactor: Effects of Feed Methane Concentration, Feed Flow Rate, Electrode Gap Distance, Residence Time, and Catalyst Distance" Applied Catalysis B: Environmental, 85, pp. 1-9, 2011.
43. Shiki H., Motoki J., Ito Y., Takikawa H., Ootsuka T., Okawa T., Yamanaka S., Usuki E., Nishimura Y., Hishida S. Sakakibara T. "Development of split gliding arc for surface treatment of conductive material", Thin Solid Films, 516, pp. 3684-3689, 2008.
44. Sun, J., Qiu, X.P., Wu, F., and Zhu, W.T. "H<sub>2</sub> from steam reforming of ethanol at low temperature over Ni/Y<sub>2</sub>O<sub>3</sub>, Ni/La<sub>2</sub>O<sub>3</sub> and Ni/Al<sub>2</sub>O<sub>3</sub> catalysts for fuel-cell application", International Journal of Hydrogen Energy, 30, pp. 437-445, 2005.
45. Vizcaino, A.J., Carrero, A., and Calles, J.A. "Hydrogen production by ethanol steam reforming over Cu-Ni supported catalysts" International Journal of Hydrogen Energy, 32, pp. 1450-1461, 2007.
46. Wang J.H., Lee C.S. Lin M.C. "Mechanism of Ethanol Reforming: Theoretical Foundations", Journal of Physical Chemistry, 113, pp. 6681-6688, 2009.
47. Wang Q., Yan B.H., Jin Y., Cheng Y. "Investigation of Dry Reforming of Methane in a

- Dielectric Barrier Discharge Reactor”, Plasma Chemical Plasma Process, 29, pp. 217-228, 2009.
48. White C.M., Steeper R.R., Lutz A.E. “The hydrogen-fueled internal combustion engine a technical review”, Intional Journal of Hydrogen Energy, 31, pp. 1292-1305, 2006.
49. Yang Y., Ma J. Wu, F. “Production of hydrogen by steam reforming of ethanol over a Ni/ZnO catalyst”, International Journal of Hydrogen Energy, 31, 877-882, 2006.
50. Yang Y.C., Lee B.J., Chun Y.N. “Characteristics of methane reforming using gliding arc reactor”, Energy, 34, pp. 172-177, 2009.
51. Zhao F., Virkar A.V. “Dependence of polarization in anode-supported solid oxide fuel cells on various cell parameters”, Journal of Power Sources, 141, pp. 79-95, 2005.



## Appendix A.

### Discussion of Gliding Arc in Tornado (GAT)

To built gliding arc in tornado (GAT) reactor, there are still a lot of details need to be concerned. For gliding arc plasma reactor, the evolution of gliding arc plasma starts at the shortest distance (usually 2-5 mm) [A. Fridman *et al.*, 2005, Z. Bo *et al.*, 2007] between two diverging electrodes when applied voltage reaches the breakdown voltage value. Immediately after breakdown, the spark channel is formed crossing the gap between the blades. However, the GA system is a two-dimensional (2D) electrode geometry causing low gas residence time in the reactor. The purpose of GAT system [A. Fridman *et al.*, 2005] is used to solve the above-mentioned drawbacks. Therefore, the GAT develop those advantages, which include: a cylindrical three-dimensional (3D) geometry which is called reverse vortex flow (Tornado), higher residence time than traditional GA.

The electrodes of GAT include three parts (In **Figure Appendix A. 1. (a)**): 1. The spiral electrode which is set and designed to harmony with the flow field shaped into tornado. 2. Circular electrode which consists of a circular electrode as anode at the top. Additionally, we hope to get the reverse vortex flow, so the GAT chamber is equipped with swirl generator (In **Figure Appendix A. 1. (b)**). The new gliding arc reactor using a



reverse vortex flow in a cylindrical chamber is called gliding arc in tornado (GAT) that contains the advantages and overcome the disadvantage of the traditional GA. The PAC system with GAT in some literatures [Nongnuch Rueangjitt, 2011] shows the excellent residence time and near-perfect thermal insulation for the reactor chamber because of the fiercely forced convection. However, the applications of GAT always is used very high flow rate ( $>10\text{slm}$ ) to push the arc along the spiral electrode in the literature surveys [Liang Yu *et al.*, 2011; Alexander F. Gutsol, 2011]. Furthermore, the results of the simulate flow field (Figure Appendix A. 2), which show most gases fast exhaust through the outlet in GAT system , caused the most fuels to be squandered. Figure Appendix A. 3 and table Appendix A. 1 show the simulate model and conditions, respectively.



## Appendix B.

### Discussion of Magnetic Gliding Arc Discharge (MGAD)

The reactor of MGAD (in [Figure Appendix B. 1](#)) is combined the magnetic around the grounded electrode with the stainless steel of power electrode which is anodic cylinder with spiral. The based principle is Ampere force which is comprised by  $I$  (Current through the conductor) cross  $V$  (Strength of magnetic force). A reactor of MAGD was built with dc power supply by S. P. Gangoli [[S.P. Gangoli \*et al.\*, 2010](#)]. Futhremore, the simulate MGAD has been accomplished in the model showed in [Figure Appendix B. 2](#) and conditions at [table Appendix B. 1](#). In the simulation, the fuel via tangentially inlet, which let the gases pass through more paths, is injected to reactor and go through the plasma region. And then the results showed that MGAD possesses more excellent residence time than gliding arc because of lower flow velocity over plasma region in [figure Appendix B. 3](#) (MGAD with 0.58 m/s, GA with ~20 m/s). However, the ethanol and water are very possible to condense at the wall without plasma region because of the closed room temperature, design carefully for this problem.

## Appendix C.

### Hydrogen Reduction Furnace

The traditional reduction method of combines the catalyst boat with the quartz of thick diameter at high temperature 600 °C and hydrogen mass flow rate of 200 SCCM in 6 hours. However, this reduction method waste a lot of costs because in base of hydrodynamics most hydrogen doesn't contact with the catalyst. For frequently using the furnace to manufacture catalyst in study, this squander should be ameliorated as soon as possible. Therefor, the new reduction furance has been design and accomplished in this study. **Figure appendix C. 1** shows interior structure of the new reduction furance in detail. First, the vertically stainless flow channel with the thin grill sieve is fixed on the pedestal. And then, the catalyst is placed on the sieve in an quartz with 41 mm of inner diameter around high temperature 650 (°C). Finally, the hydrogen goes through the catalyst and carries out the O atoms to accomplish the hydrogen reduction. **Table appendix C. 1** and **figure appendix C. 3** shows the detailed test conditions and the appearance construction respectively. In the preliminary test using  $\text{Ni}_{0.35}\text{Mg}_{2.65}\text{FeO}_{4.5}$  catalyst, the successful outcomes shows that the new system economize on hydrogen mass flow very well rate during the reducion process (**figure appendix C. 2**).

**TABLE**

Catalyst (wt %)	Carrier	T (°C)	Conversion Rate (%)	H <sub>2</sub> Selectivity (%)	Reference
Rh (1)	$\gamma$ -Al <sub>2</sub> O <sub>3</sub>	750	100	~95	Liguras 2003
Rh (2)			100	~96	
Ru (1)			42	~55	
Ru (5)			100	~96	
Pt (1)			60	~65	
Pd (1)			55	~50	
Rh (3)	MgO	650	99	91	Frusteri 2004
Pd (3)			10	70	
Ni (21)			42	97	
Co (21)			55	92	
Ru (1)	CeO <sub>2</sub>	450	56(20min) 25(100min)	35(20min) 24(100min)	Erdohelyi 2006
Rh (1)			80(20min) 57(100min)	83(20min) 72(100min)	
Ir (1)			54(20min) 35(80min)	40(20min) 25(80min)	
Pt (1)			89(20min) 88(100min)	35(20min) 40(100min)	
Pd (1)			33(20min) 25(100min)	32(20min) 18(100min)	
Rh (2)	CeO <sub>2</sub>	300	58.5	59.7	Diagne 2004
		400	100	66.3	
		500	100	69.1	
	ZrO <sub>2</sub>	300	100	57.4	
		400	100	68.1	
		500	100	71.7	

**Table 1.1:** Properties of ethanol steam reforming with different noble metal catalysts.



Catalyst (wt %)	Carrier	T (°C)	Conversion Rate (%)	H <sub>2</sub> Selectivity (%)	Reference
Ni (20)	La <sub>2</sub> O <sub>3</sub>	773	35	70	Fatsikostas 2004
		1073	~100	95	
	γ-Al <sub>2</sub> O <sub>3</sub>	973	77	87	
		1073	100	96	
Ni (20.6)	Y <sub>2</sub> O <sub>3</sub>	593	93	50 (60hr)	Sun 2005
Ni (16.1)	γ-Al <sub>2</sub> O <sub>3</sub>		89	44.4(60hr)	
Ni (15.3)	La <sub>2</sub> O <sub>3</sub>		100	62.3(60hr)	
Ni (35)	γ-Al <sub>2</sub> O <sub>3</sub>	773	100	91	Comas 2006
Ni <sub>0.35</sub> Mg <sub>2.65</sub> FeO <sub>4.5</sub>	Al <sub>2</sub> O <sub>3</sub>	973	100	46.7	Li 2010
Ni (10)	γ-Al <sub>2</sub> O <sub>3</sub>	923	100	78.2	Yang 2006
	MgO		100	82.2	
	La <sub>2</sub> O <sub>3</sub>		100	89.3	
	ZnO		100	89.1	
Ni (21)	MgO	923	45(20hr)	95(20hr)	Frusteri 2004
K(1)-Ni(21)			59(20hr)	93(20hr)	
Na(1)-Ni(21)			55(20hr)	95(20hr)	
Li(1)-Ni(21)			83(20hr)	91(20hr)	
Cu(2)-Ni(14)	SiO <sub>2</sub>	873	100	71.5	Vizcaño 2007
Cu(2)-Ni(14)	Al <sub>2</sub> O <sub>3</sub>		99.2	50.1	
Co (10)	ZnO	623	100(75hr)	73.4	Llorca 2003
Co(10)-Na(0.06)	ZnO	673	100	72.1	Llorca 2004b
Co(10)-Na(0.23)			100	73.4	
Co(10)-Na(0.78)			100	74.2	
Co(10)-Na(0.06)		723	100	73.1	
Co(10)-Na(0.23)			100	73.7	
Co(10)-Na(0.78)			100	74.0	

**Table 1.2:** Properties of ethanol steam reforming with different non-noble metal catalysts.

Author	Type	Fuel	Flow Rate (SLM)	Performance			
				Plasma Power (W)	<sup>1</sup> C (%)	<sup>2</sup> S (%)	<sup>3</sup> E (%)
A. Fridman <i>et al.</i> (2005)	GA	CH <sub>4</sub>	2-10	200	75	N/A	75.81
	GAT	CH <sub>4</sub> H <sub>2</sub> S	5-20	~2,700	80	N/A	74
L. Bromberg <i>et al.</i> (2006)	GEN2	EtOH	30	200	80.9	N/A	46.67
Y. N. Chun <i>et al.</i> (2008)	GA	C <sub>3</sub> H <sub>8</sub>	11-20	1300	63	N/A	N/A
J. Yan <i>et al.</i> (2008)	GA	CH <sub>4</sub> + CO <sub>2</sub>	13	200-500	40	40-70	N/A

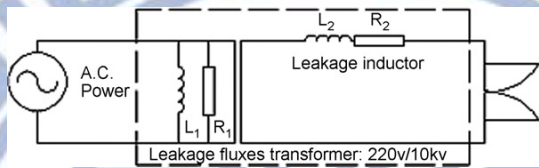
1. C: conversion rate 2. S: selectivity 3. E: efficiency

**Table 1.3:** Summary of important features, experiments and parameters for plasma alone reforming.

Author	Catalyst	Type	Fuel	Flow Rate (SLM)	Performance			
					Plasma Power (W)	<sup>1</sup> C (%)	<sup>2</sup> S (%)	<sup>3</sup> E (%)
M.B. Chang <i>et al.</i> (2008)	Ni	GA	CH <sub>4</sub>	5-10	35	90	98	N/A
Y. N. Chun <i>et al.</i> (2008)	Ni	GA	CH <sub>4</sub>	5-30	1300	~100	93	35
Y. N. Chun & H.O. Song <i>et al.</i> (2008)	Ni	GA	C <sub>3</sub> H <sub>8</sub> +CO <sub>2</sub> +H <sub>2</sub> O	14	1370	60-80	N/A	N/A
H.S. Sekiguchi <i>et al.</i> (2009)	Ru	GA	Isooctane	0.2	12	75	25-45	N/A
G. Mallinson (2010)	Pt	Cornona	EtOH+H <sub>2</sub> O	0.6	15	~100	180	N/A

1. C: conversion rate 2. S: selectivity 3. E: efficiency

**Table 1.4:** Summary of important features, experiments and parameters for PAC.

Author	Phase	Power generator	Power input
Y. Kusano <i>et al.</i> (2008)	AC	Power supply (Generator 6030. SOFTAL Electronic GmbH, Germany).	Input power: 1.6-2.2 kW  Frequency: 33-40 kHz
B. Zheng <i>et al.</i> (2008)	AC		Input voltage: 10 kV  Frequency: 50 Hz
A.Fridman <i>et al.</i> (2005-2010)	DC	Power supply (Universal Voltronics, Inc.)	Input voltage: 10 kV  Input current: 0.05-0.15 A
H. Shiki <i>et al.</i> (2008)	Pulse	<p>Pulse modulator (Kurita Seisakusho Co., Ltd., 6 kW)</p> <p>Slide regulator (Matsunaga Seisakusho, S3-2413, 5.2 kVA)</p> <p>High-voltage transformer (Kurita Seisakusho Co., Ltd., 250/12 kV)</p>	<p>Input power: 300 W</p> <p>Pulse frequency: 15-20 kHz</p> <p>Pulse width: 1.6-2.8 <math>\mu</math>s</p>

**Table 1.4:** Summary of plasma power input type.



Reforming	Fuel	C/O Ratio	Catalyst	Plasma Power (W)	Reactor temperature (°C)
Gliding Arc	Ethanol/water 33.33 mol% with air, 0.5-2.0 SLM	0.3-0.8	N/A	223	Gasification: 160 Furnace: 230
Catalyst	Ethanol/water 33.33 mol% with air, 0.5-2.0 SLM	0.7	5 wt% a Rh/CeO <sub>2</sub> /Al <sub>2</sub> O <sub>3</sub>	N/A	Gasification: 160 Furnace: 230
PAC with gliding arc	Ethanol/water 33.33 mol% with air, 0.5-2.0 SLM	0.7	5 wt% Rh/CeO <sub>2</sub> /Al <sub>2</sub> O <sub>3</sub>	223	Gasification: 160 Furnace: 230

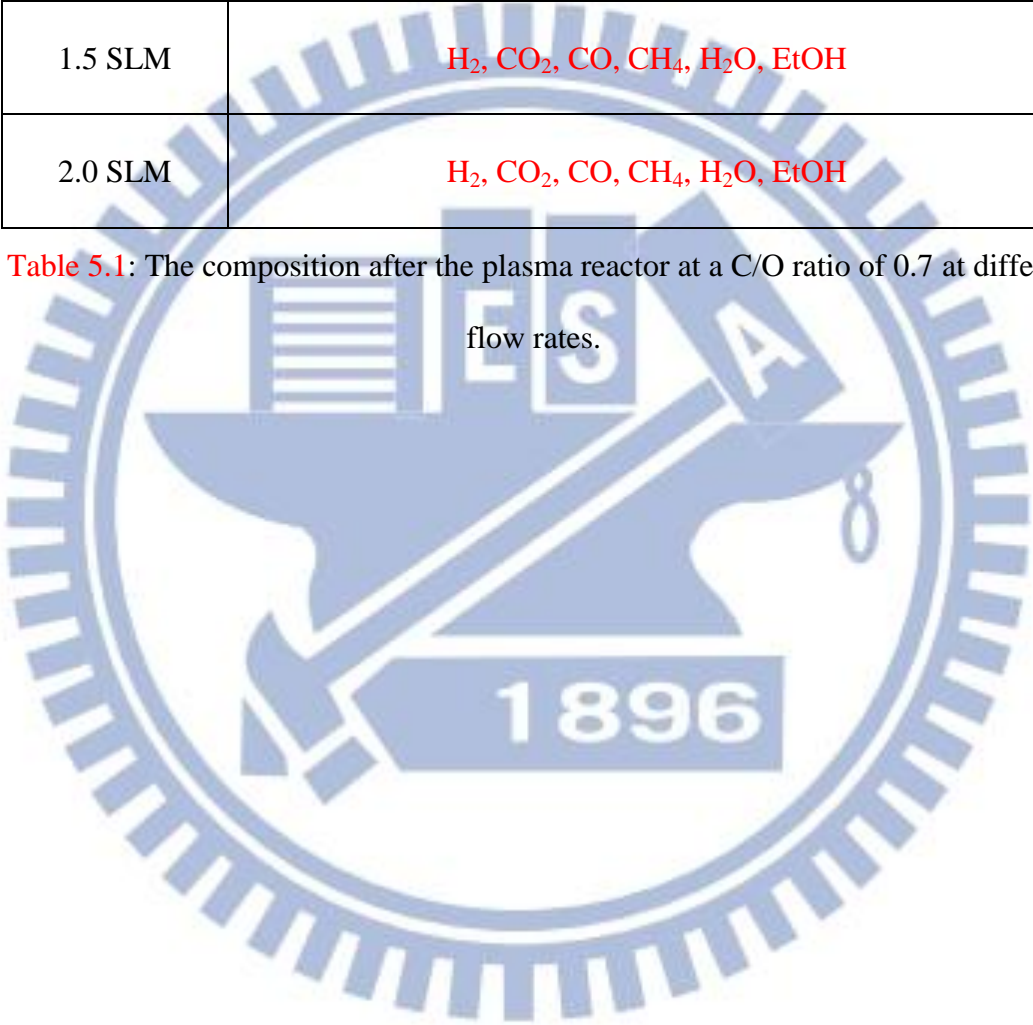
**Table 3.1:** Test Condition of gliding arc, catalyst(Rh/CeO<sub>2</sub>/Al<sub>2</sub>O<sub>3</sub>), PAC with gliding arc reforming

Reforming	Fuel	C/O Ratio	Catalyst	Plasma Power (W)	Reactor temperature (°C)
Catalyst	Ethanol/water 33.33 mol% with air, 1.0 SLM	0.7	10 wt% Ni <sub>0.35</sub> Mg <sub>2.65</sub> Fe <sub>0.45</sub> /Al <sub>2</sub> O <sub>3</sub>	N/A	Gasification: 160 Furnace: 200-400
PAC with gliding arc	Ethanol/water 33.33 mol% with air, 1.0 SLM	0.7	10 wt% Ni <sub>0.35</sub> Mg <sub>2.65</sub> Fe <sub>0.45</sub> /Al <sub>2</sub> O <sub>3</sub>	223	Gasification: 160 Furnace: 200

**Table 3.2:** Test Conditions of catalyst (Ni<sub>0.35</sub>Mg<sub>2.65</sub>Fe<sub>0.45</sub>), PAC with gliding reforming

Air Flow Rate	Compositions
0.5 SLM	H <sub>2</sub> , CO <sub>2</sub> , CO, CH <sub>4</sub> , C <sub>2</sub> H <sub>4</sub> (trace), C <sub>2</sub> H <sub>6</sub> (trace), H <sub>2</sub> O, EtOH
1.0 SLM	H <sub>2</sub> , CO <sub>2</sub> , CO, CH <sub>4</sub> , H <sub>2</sub> O, EtOH
1.5 SLM	H <sub>2</sub> , CO <sub>2</sub> , CO, CH <sub>4</sub> , H <sub>2</sub> O, EtOH
2.0 SLM	H <sub>2</sub> , CO <sub>2</sub> , CO, CH <sub>4</sub> , H <sub>2</sub> O, EtOH

**Table 5.1:** The composition after the plasma reactor at a C/O ratio of 0.7 at different air flow rates.



The Simulate conditions in GAT	
Parameter	Range
MFR (SLM)	2
IA(°)	0°-30°
B.C	Outlet : 101,300 Pa = 1 atm Wall : Stationary Wall
I.C	101,300 Pa = 1 atm
Gravity ( $M/S^2$ )	-9.8
Number of Mesh	500,000
Number of Iterations	2,000

1. MFR: Mass Flow Rate 2. IA: Injected Angle 3. B.C.: Boundary Conditions 4. I.C.: Initial Condition

**Table Appendix A. 1:** The parameters for simulation of gliding arc in tornado.

<b>The Simulate conditions in MGAD</b>	
<b>Parameter</b>	<b>Range</b>
<b>MFR (SLM)</b>	2
<b>B.C</b>	<i>Outlet : 101,300 Pa = 1 atm Wall : Stationary Wall</i>
<b>I.C</b>	<i>101,300 Pa = 1 atm</i>
<b>Gravity (<math>M/S^2</math>)</b>	-9.8
<b>Number of Mesh</b>	500,000
<b>Number of Iterations</b>	2,000

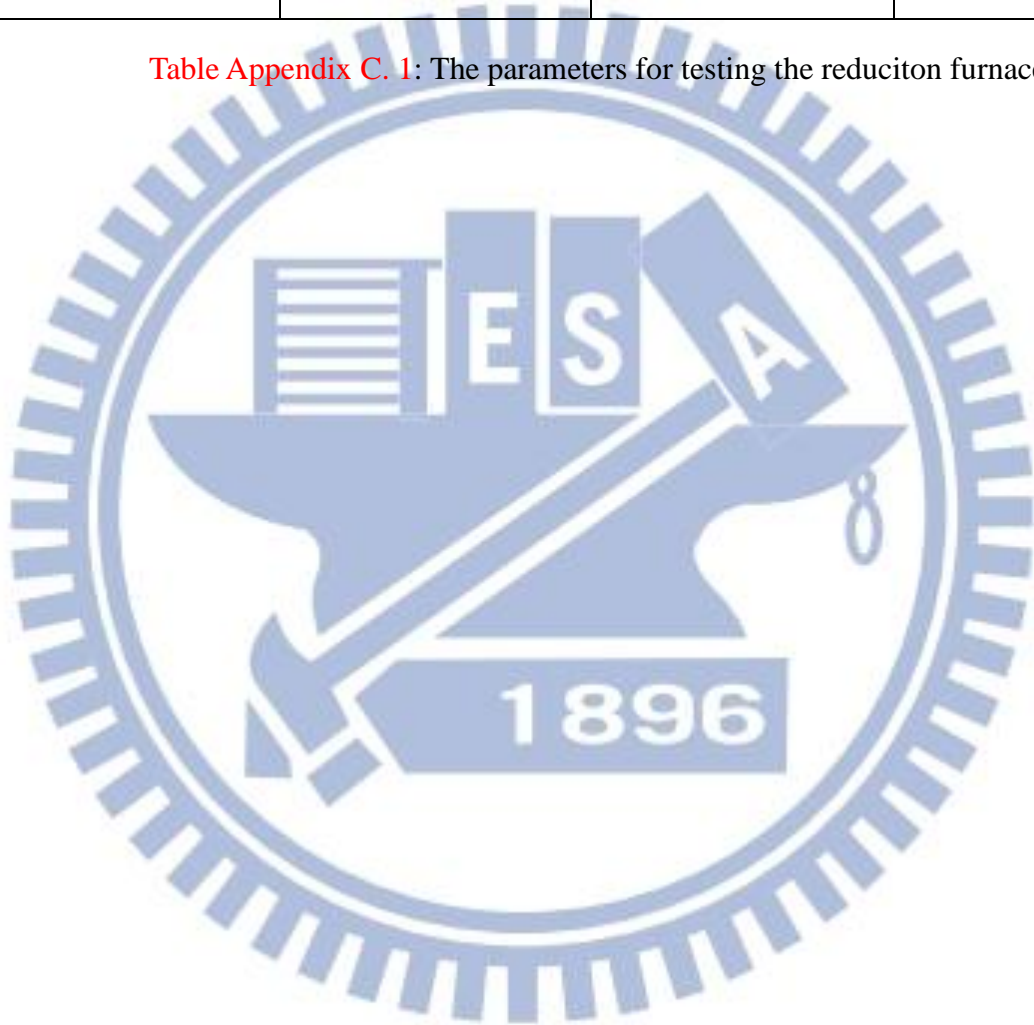
1. MFR: Mass Flow Rate 2. IA: Injected Angle 3. B.C.: Boundary Conditions 4. I.C.: Initial Condition

**Table Appendix B. 1:** The parameters for simulation of magnetic gliding arc discharge.



Test	Reduction Time (hr)	H <sub>2</sub> Flow Rate (SCCM)	Furnace Temperature (°C)
Sample 1	5	50	650
Sample 2	2	30	650
Sample 3	0.5	30	650

**Table Appendix C. 1:** The parameters for testing the reduciton furnace.



## FIGURE

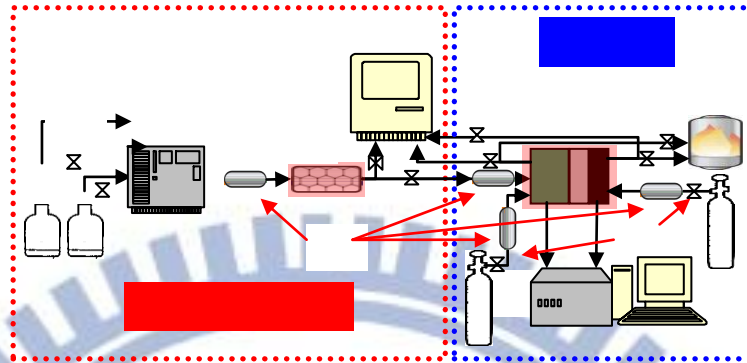


Figure 1.1: Sketch of the typical test arrangement for ethanol reformer (left) and the SOFC (right) at CGET of NCTU.

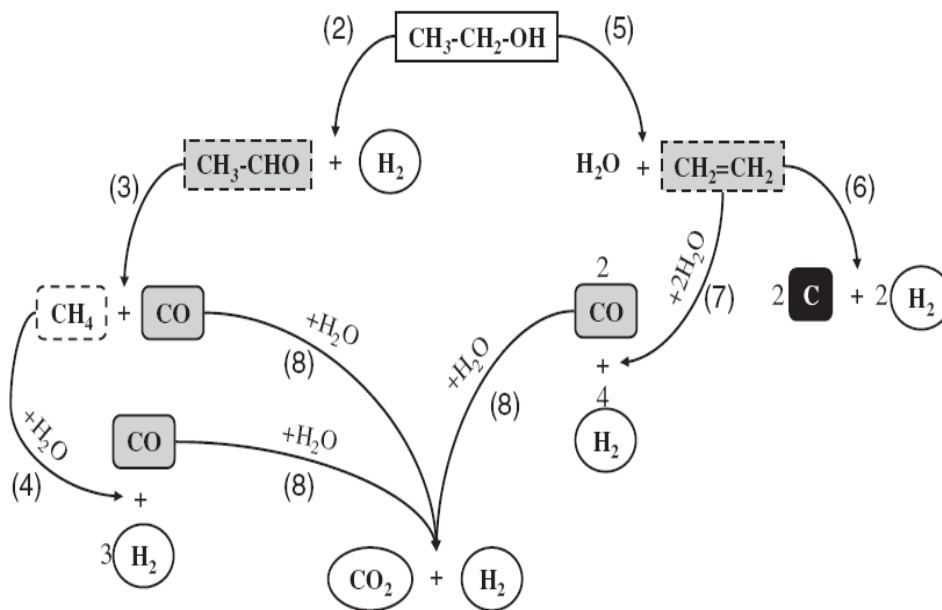


Figure 1.2: The basic reaction of ethanol steam reforming [Vizcaino *et al.*, 2007].

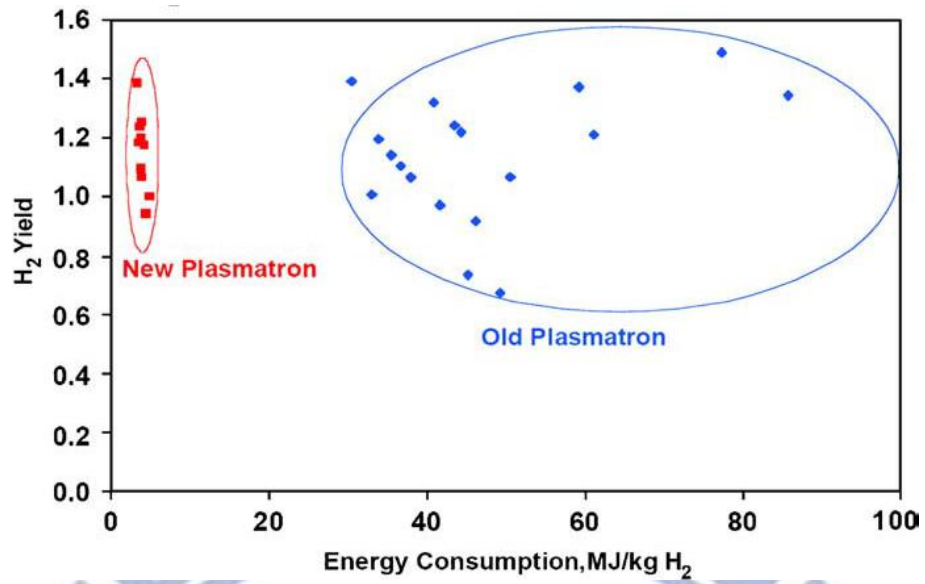


Fig. 1.3: Comparisons of yields for non-thermal (new plasmatron) and thermal (old plasmatron) plasmas [G. Petipas, *et al.*, 2007].

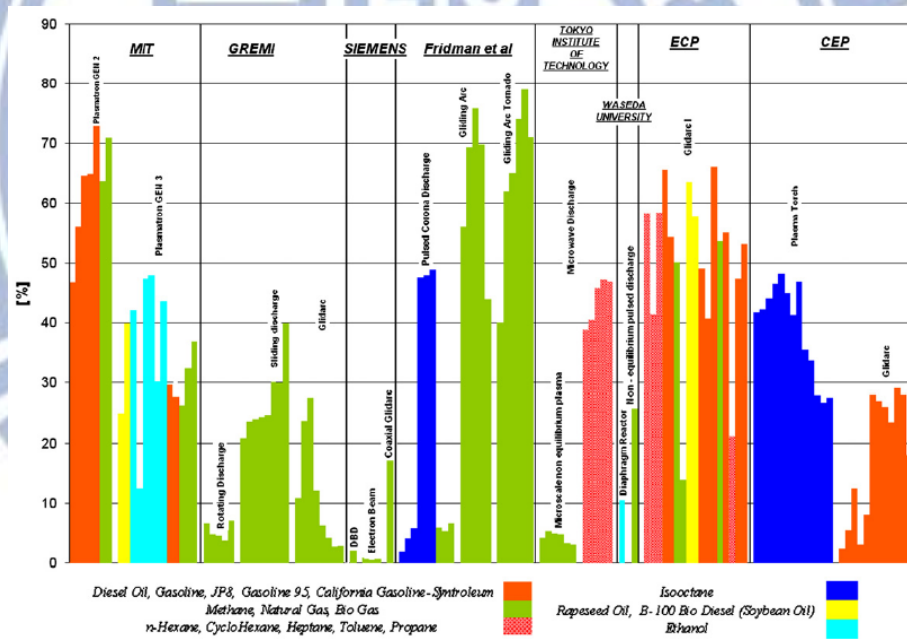
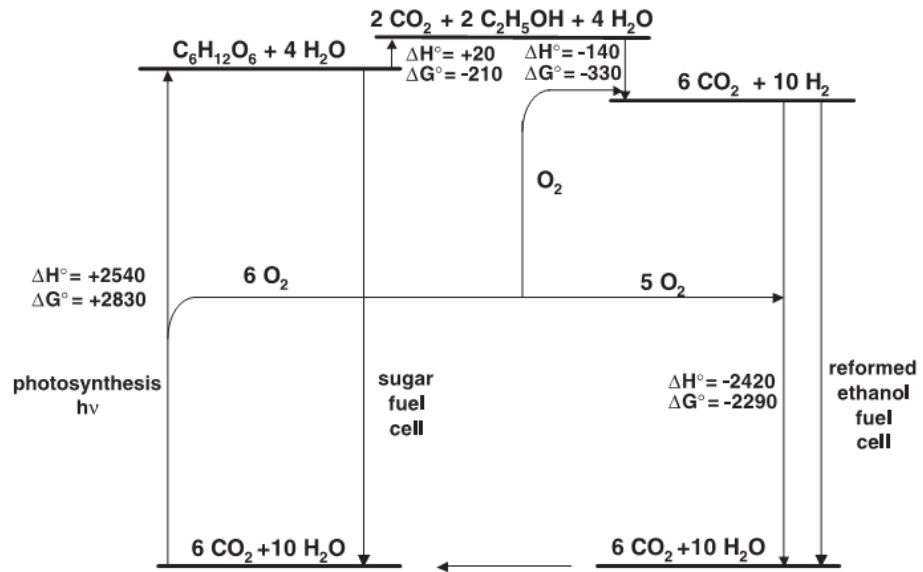
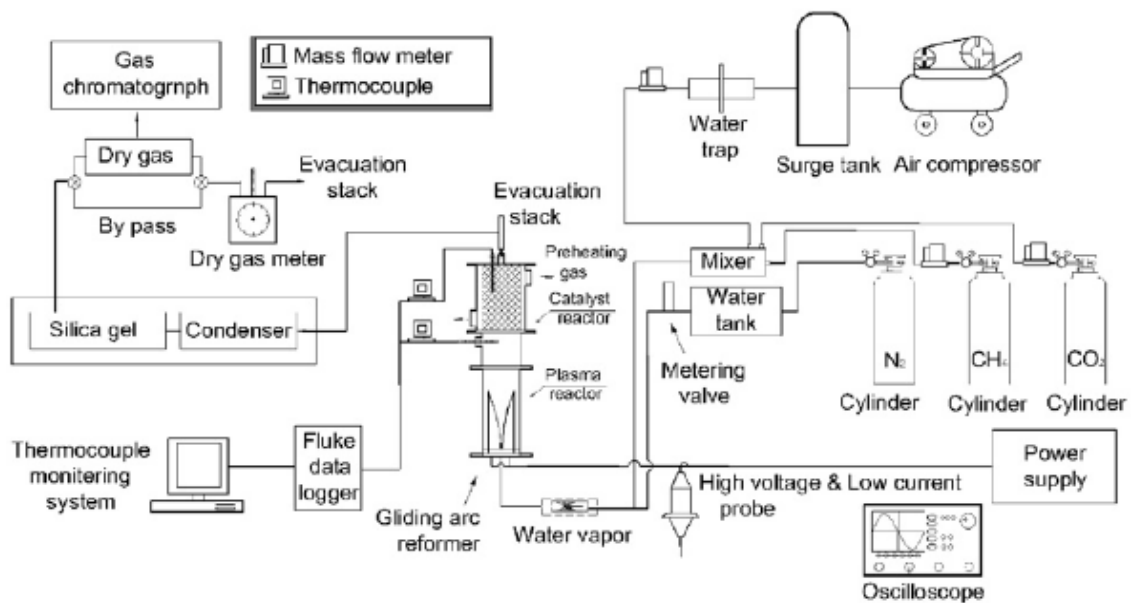


Fig. 1.4: The comparison between different plasma reactors [G. Petipas, *et al.*, 2007].



**Figure 1.5:** An energy diagram indicating the standard enthalpy ( $\Delta H^\circ$ ) and free energy changes ( $\Delta G^\circ$ ) in kJ/mol for the reactions in a renewable energy cycle operating between CO<sub>2</sub> and biomass [L. D. Schmidt, *et al.*, 2004].



**Figure 1.6:** Typical arrangement of instrumentation for PAC system [Y. C. Yang *et al.*, 2009].



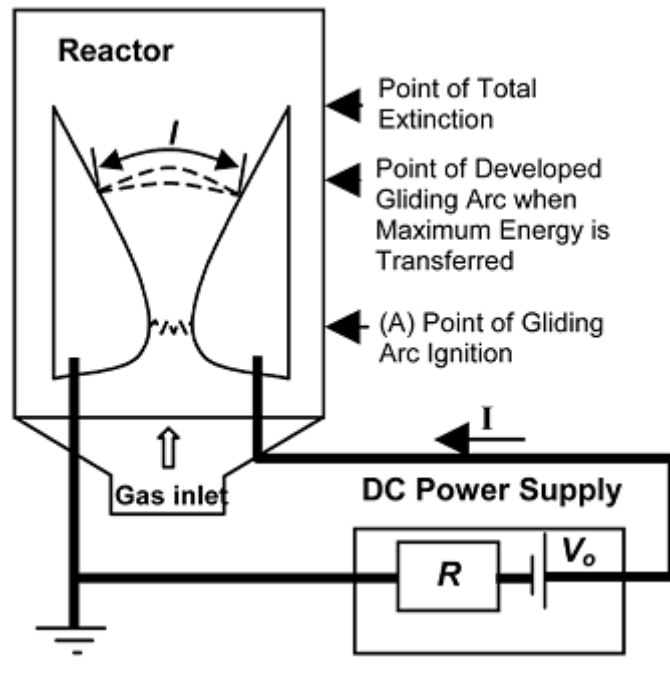


Figure 2.1: Schematic of gliding arc reactor. [A. Fridman *et al.*, 2002].

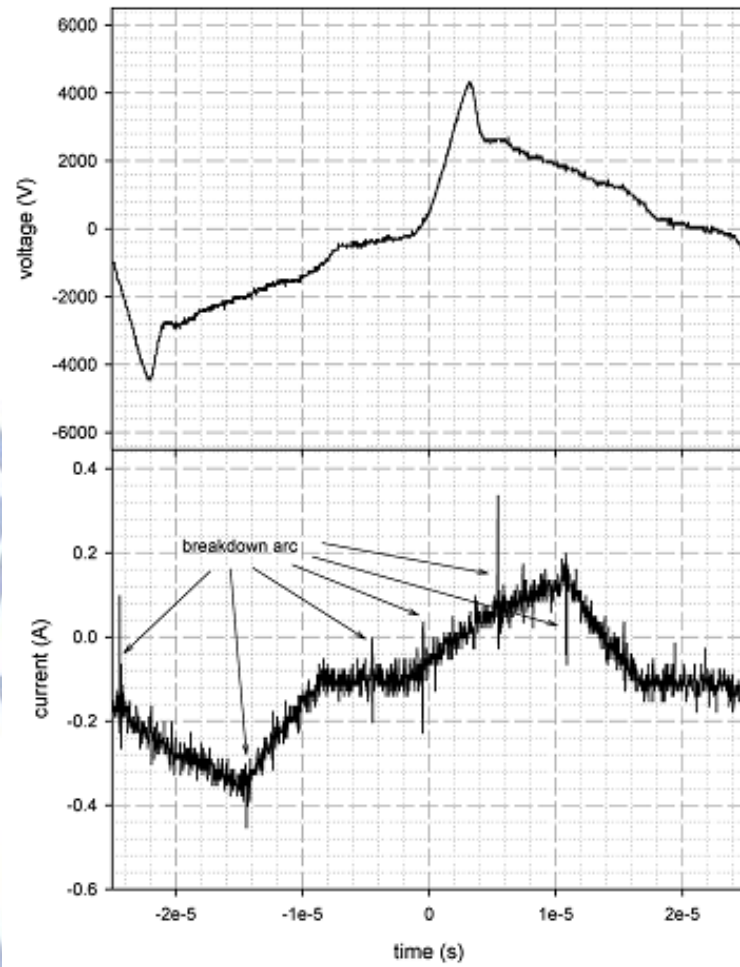


Figure 2.2: (a) voltage waveform of gliding arc production; (b) current waveform of gliding arc production [Antonius I. *et al.*, 2006].

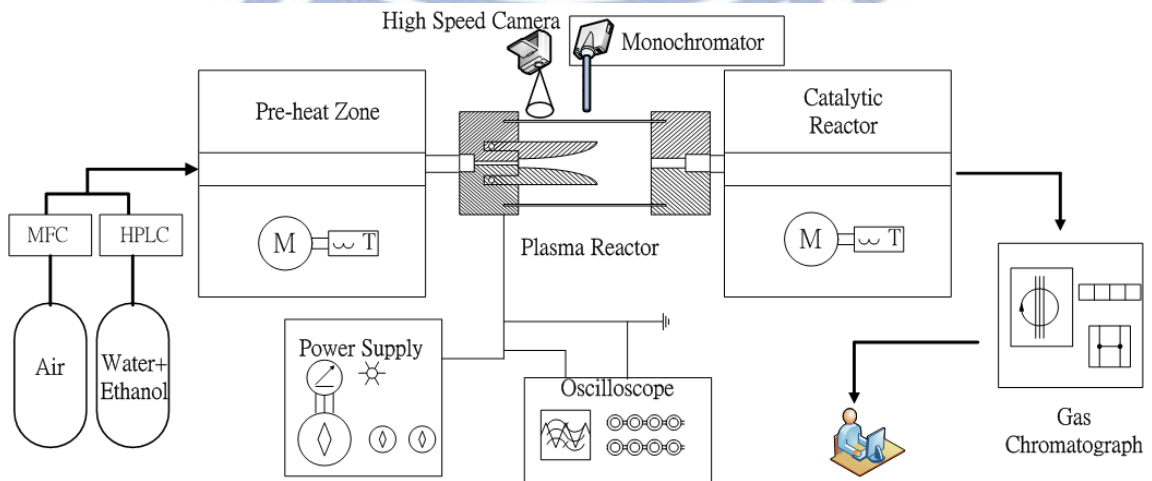
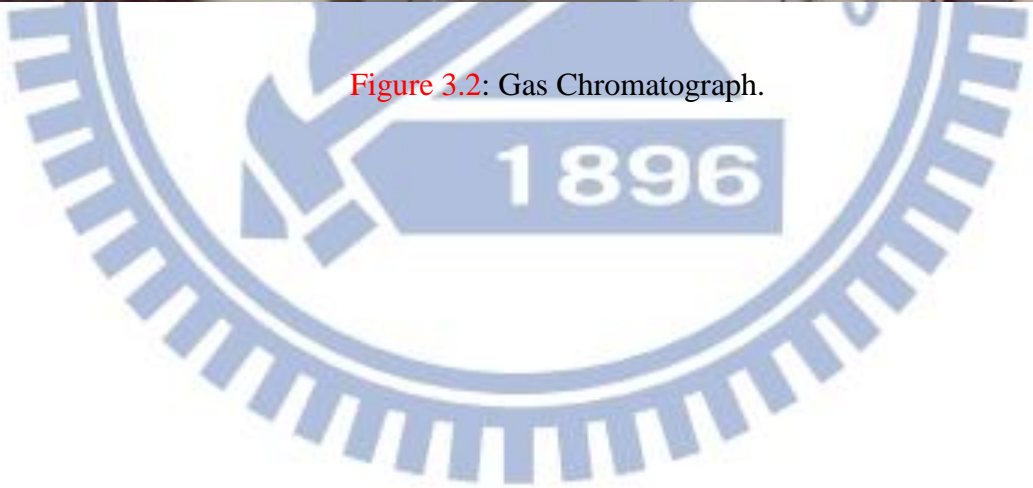
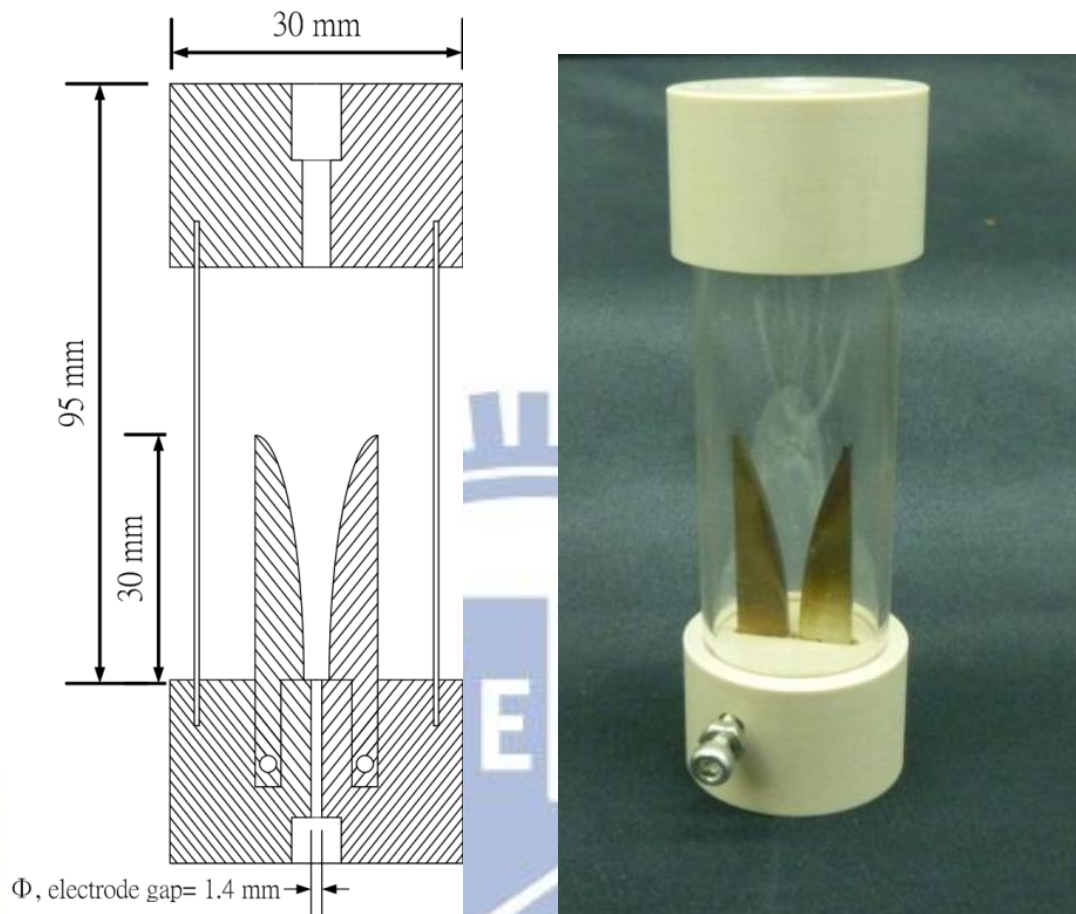


Figure 3.1: The experimental arrangement of PAC system.



Figure 3.2: Gas Chromatograph.





**Figure 3.3:** The self-designed gliding arc reactor.



**Figure 3.4:** PVM500 plasma driver





Figure 3.5: The MFC and liquid pump.



Figure 3.6: The fuel Injections



Figure 3.7: The furnaces for heating system

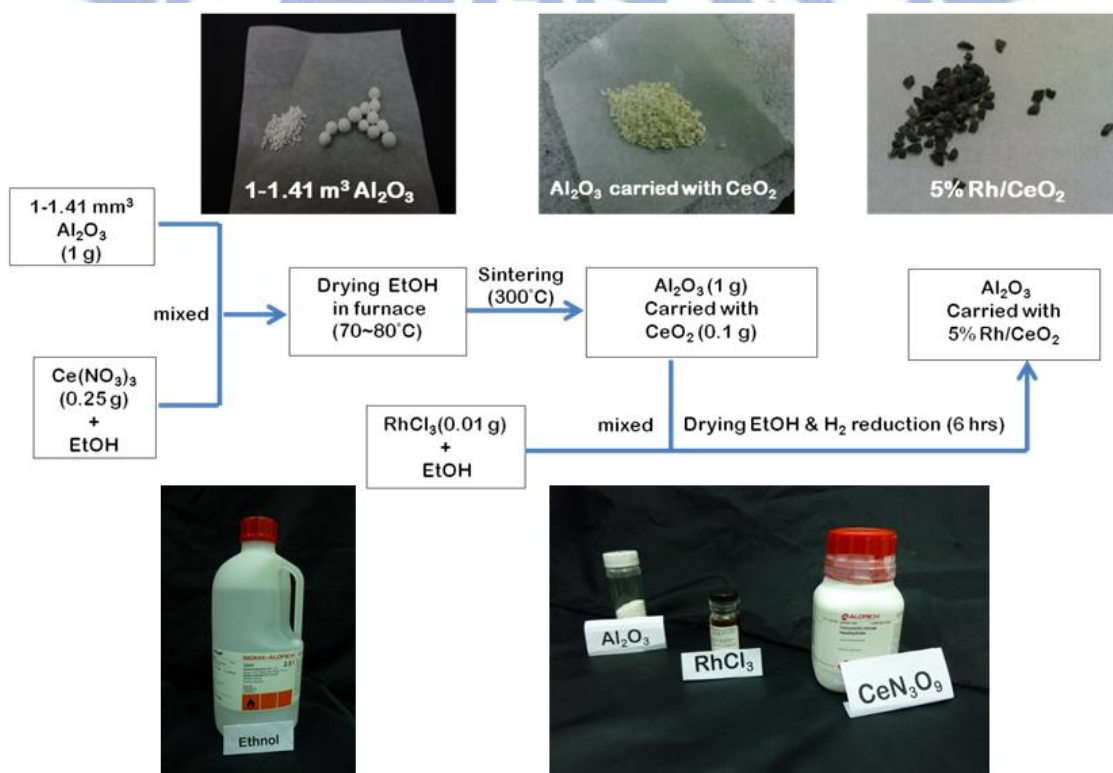


Figure 3.8: The Rh catalyst setup procedure.

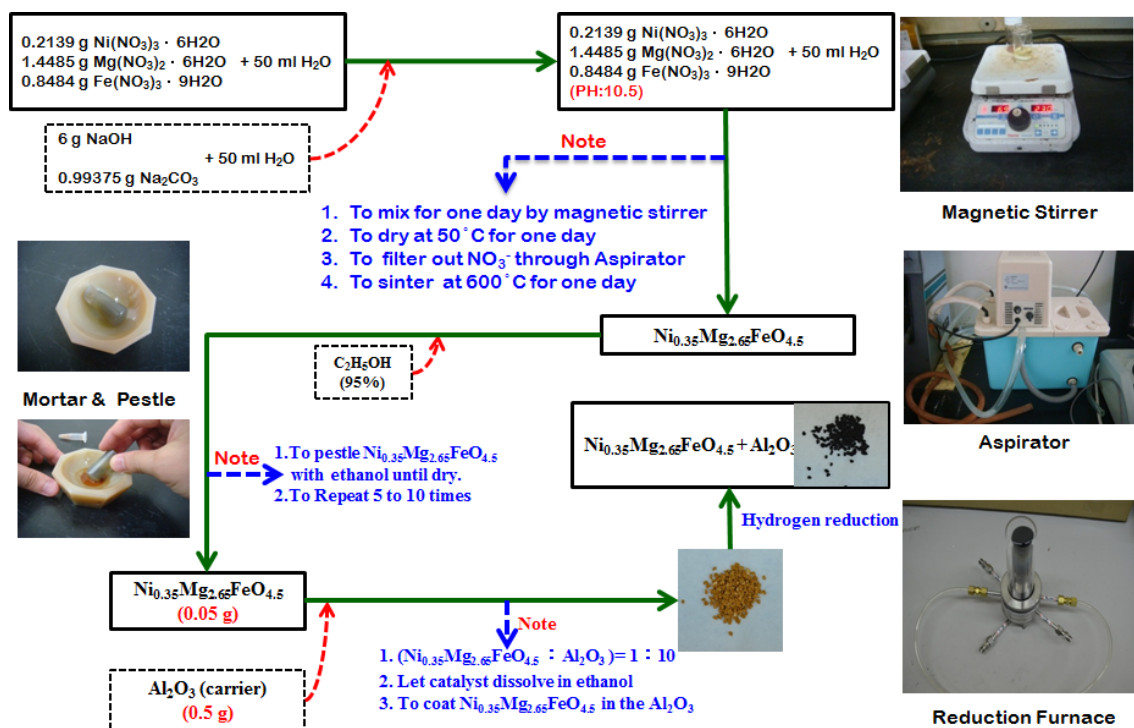


Figure 3.9: The  $\text{Ni}_{0.35}\text{Mg}_{2.65}\text{FeO}_{4.5}$  catalyst setup procedure



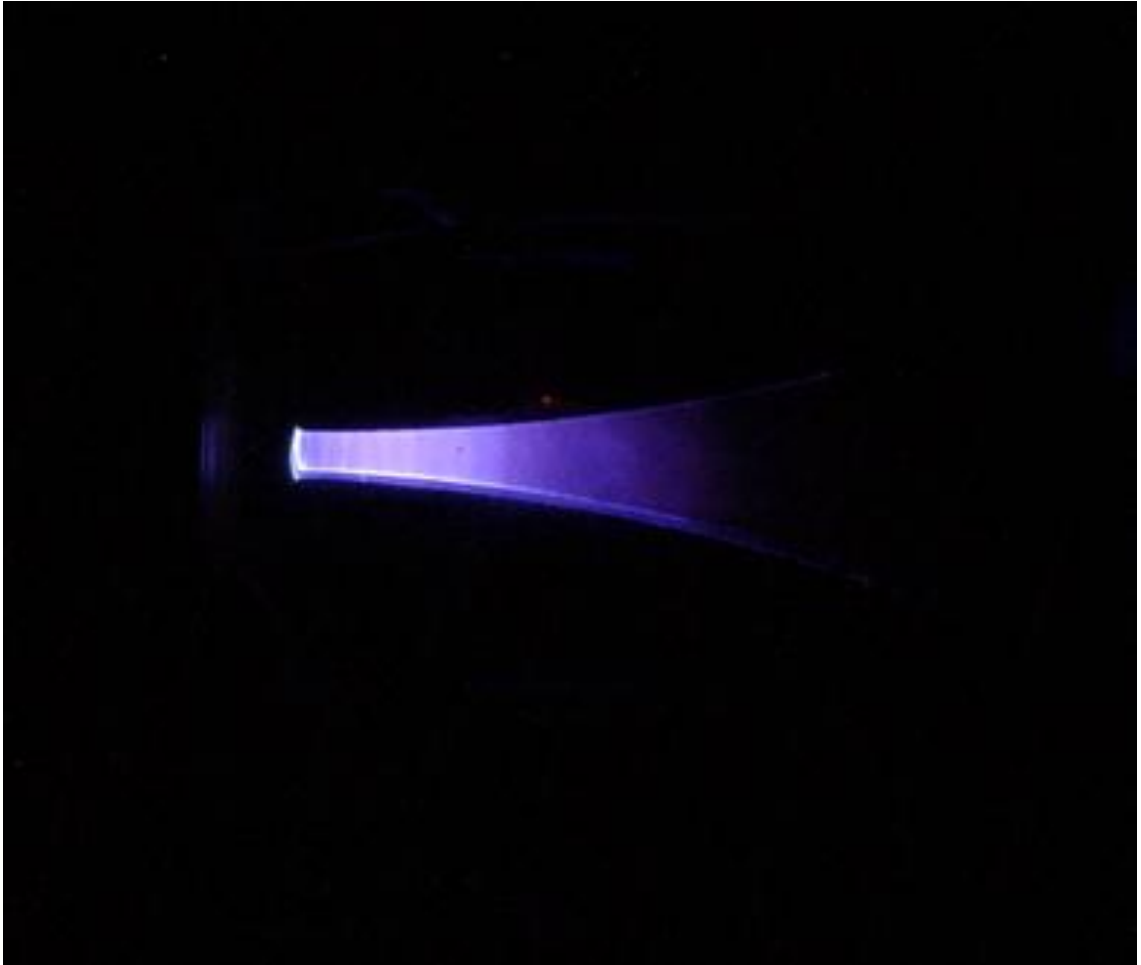
Figure 3.9: High-voltage probe.



Figure 3.10: Rogowski coil and Oscilloscope.







**Figure 4.1:** The visualization of gliding arc discharge. The parameters: air flow rate is 1..5

SLM; The plasma power from power supply is 223 W with 20 kHz

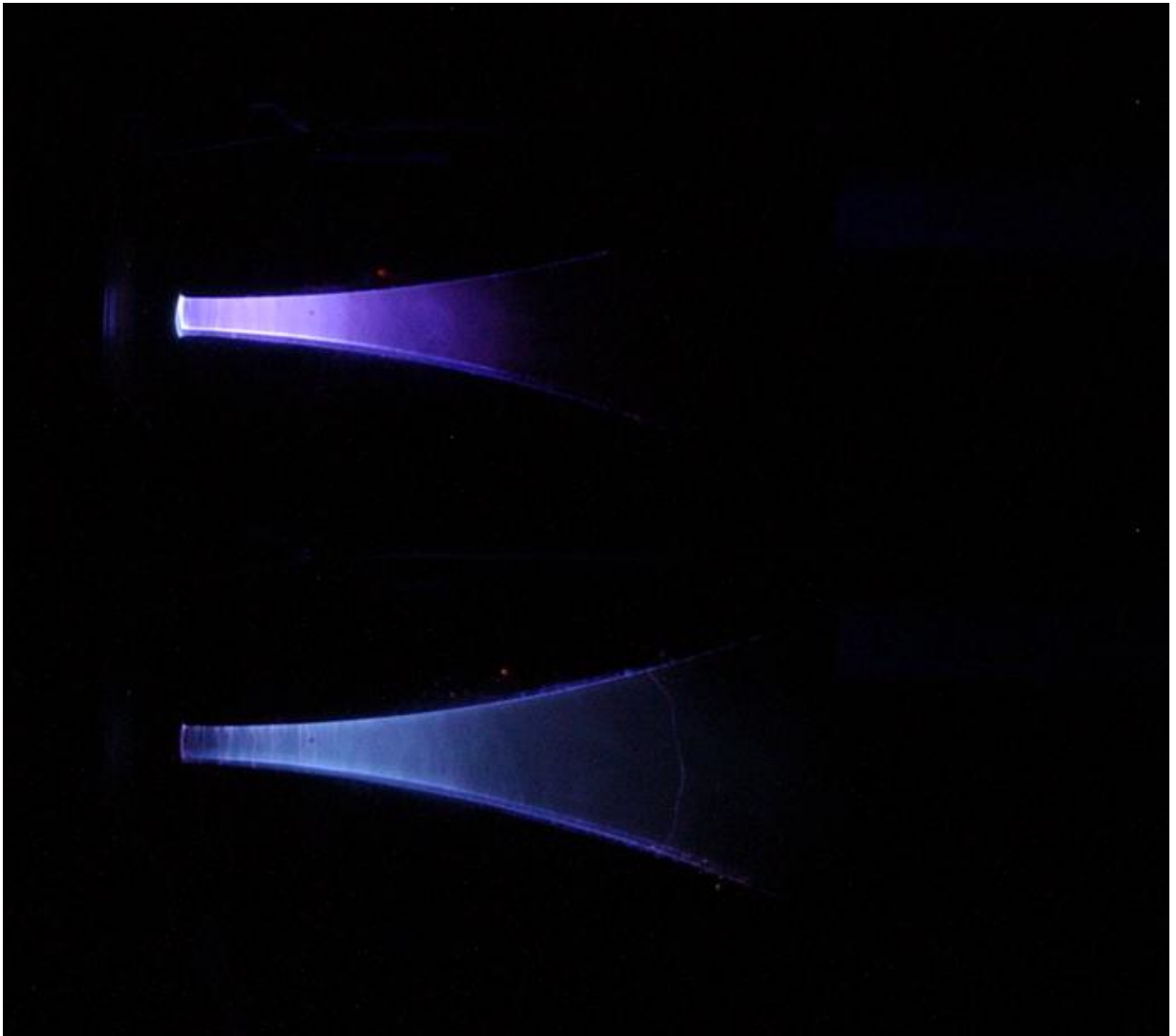


**Figure 4.2:** The visualization of comparison of the gliding arc with C/O ratio or not.

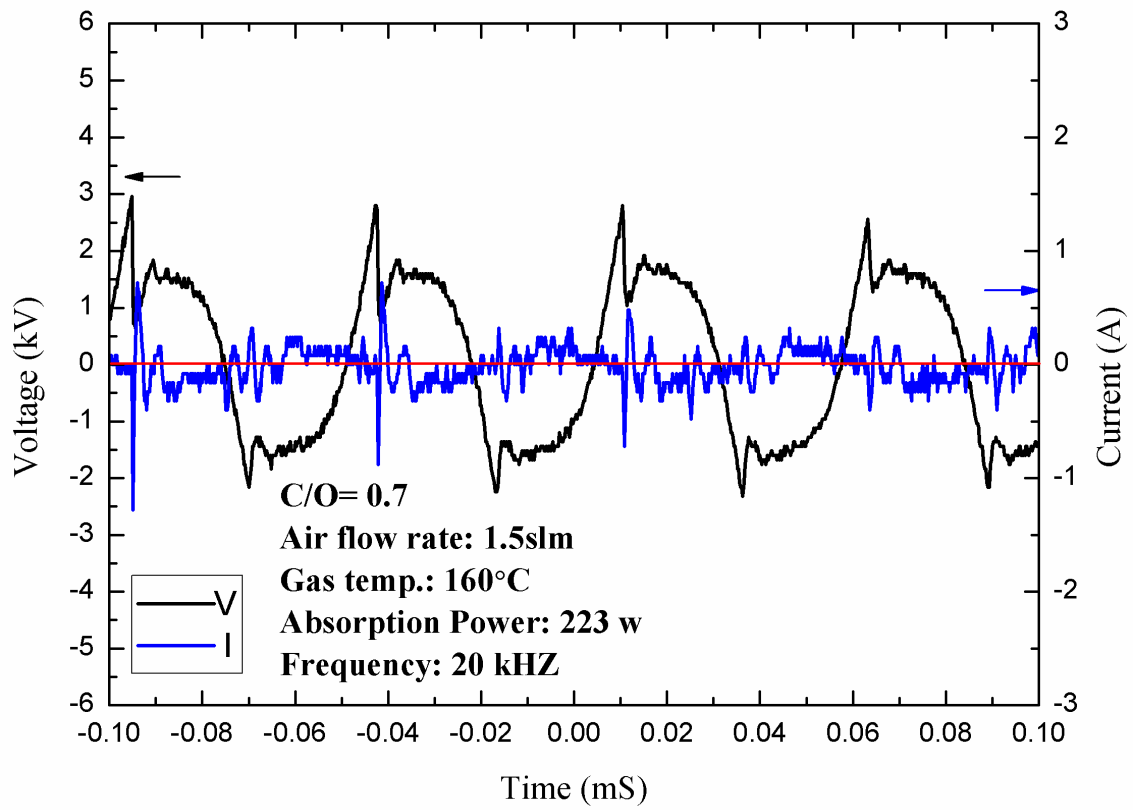
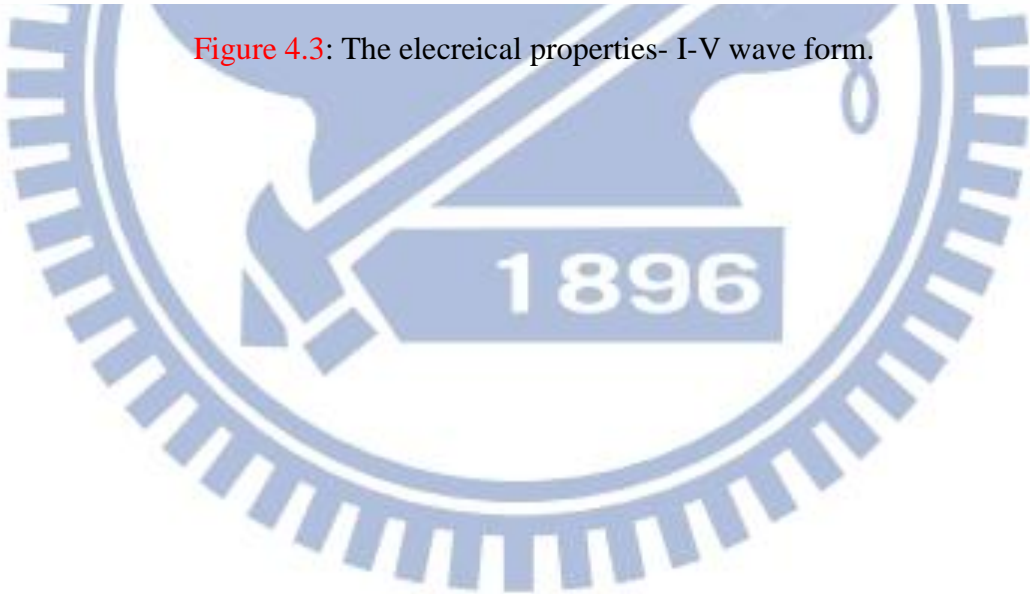


Figure 4.3: The electrical properties- I-V wave form.



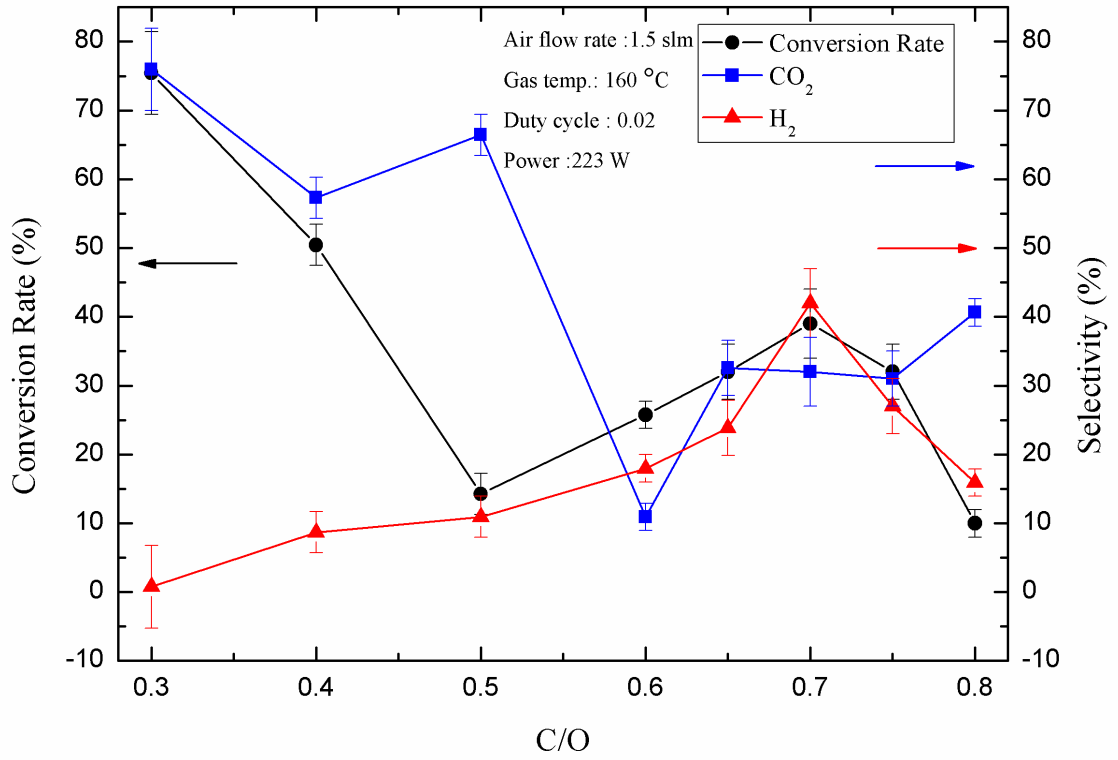
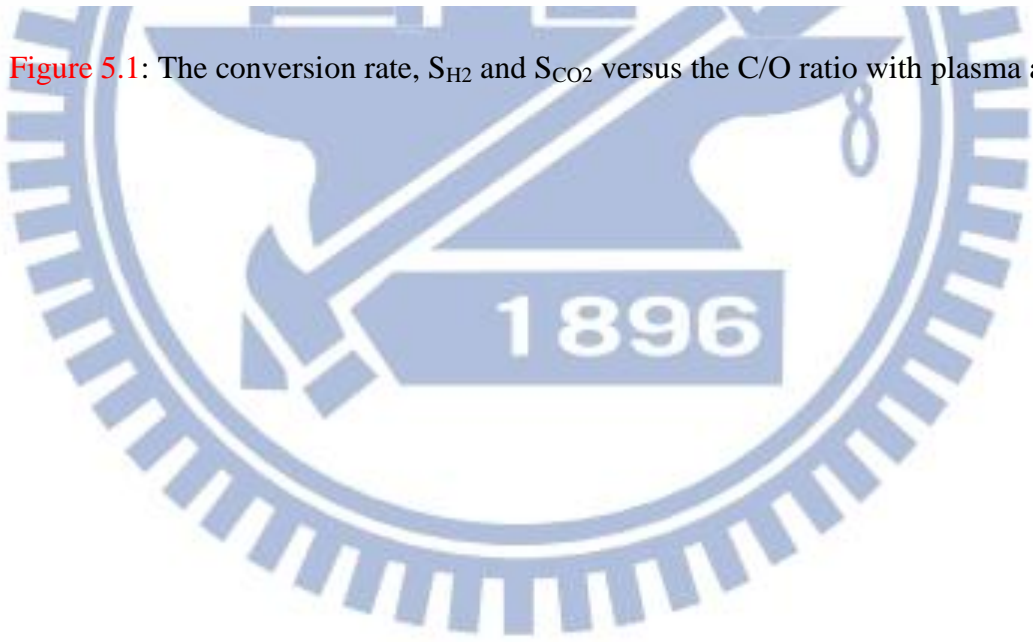
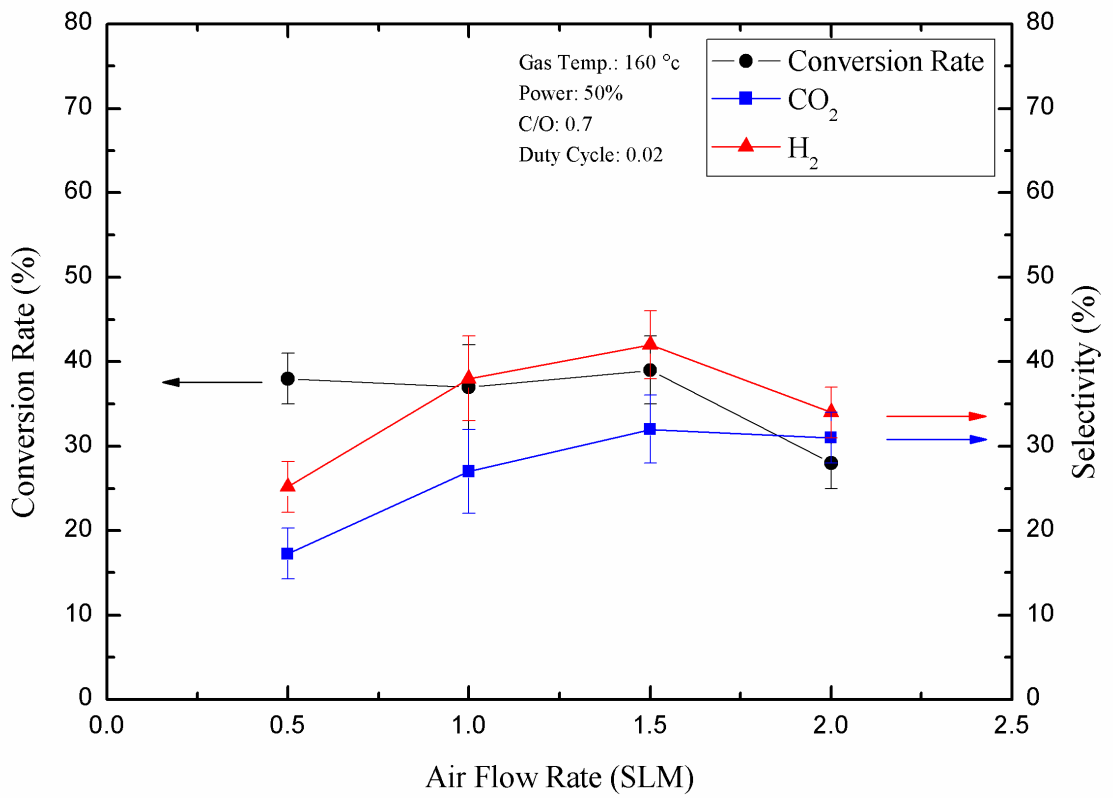


Figure 5.1: The conversion rate,  $S_{H_2}$  and  $S_{CO_2}$  versus the C/O ratio with plasma alone.







**Figure 5.2:** The conversion rate,  $S_{H_2}$  and  $S_{CO_2}$  as functions of the air flow rate with plasma alone at a C/O ratio of 0.7.

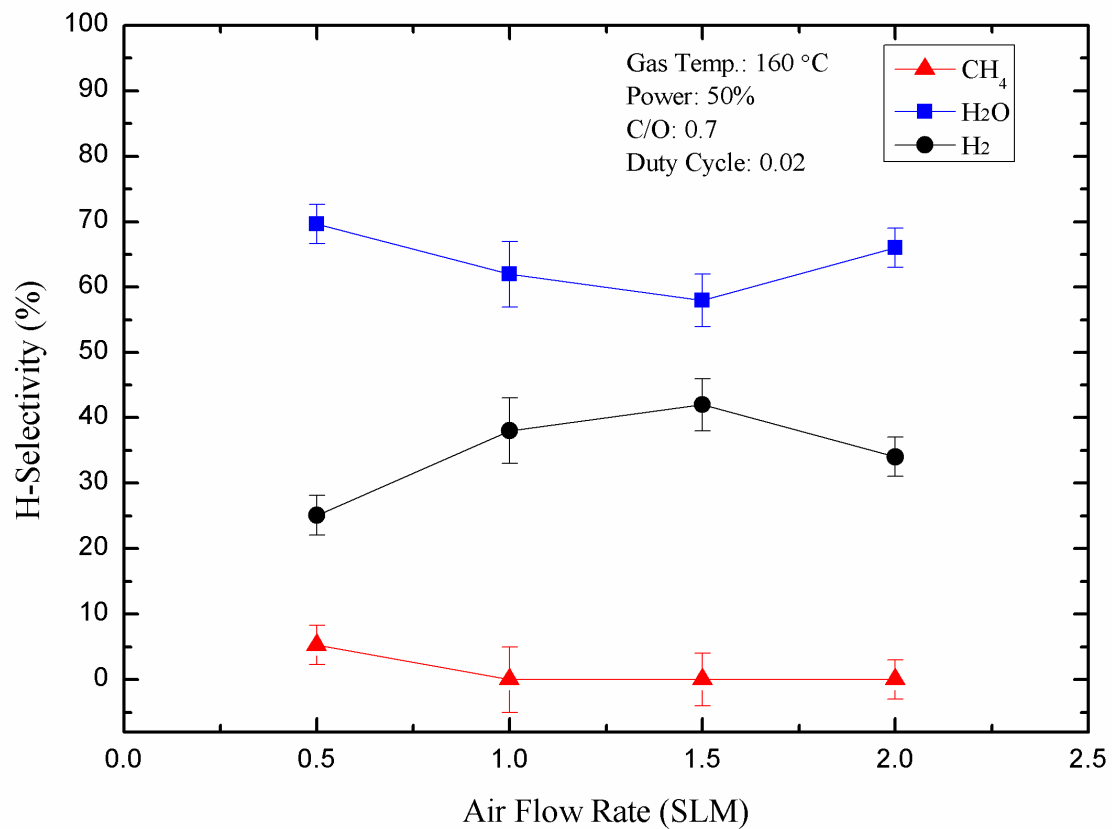
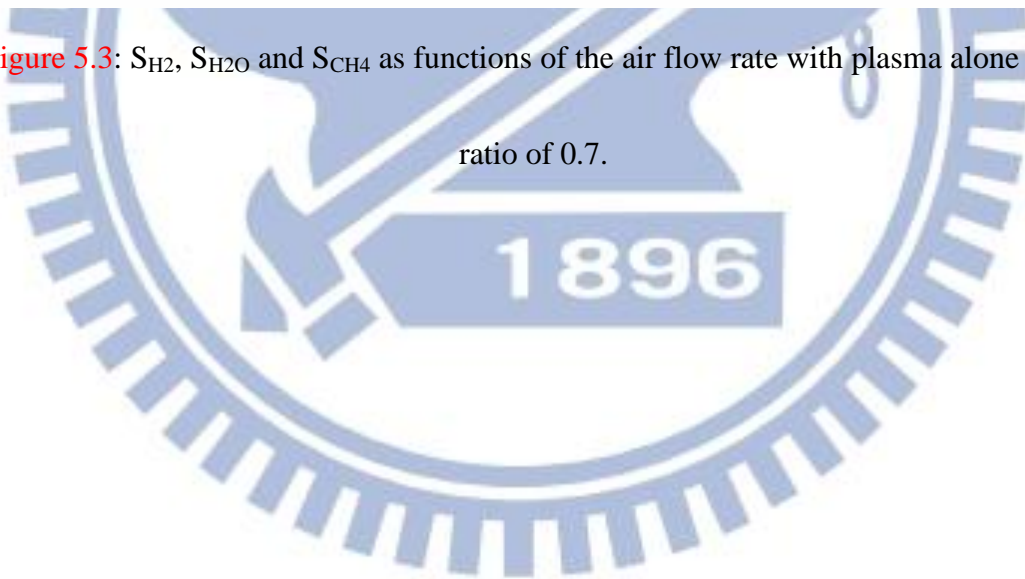


Figure 5.3:  $S_{H_2}$ ,  $S_{H_2O}$  and  $S_{CH_4}$  as functions of the air flow rate with plasma alone at a C/O ratio of 0.7.



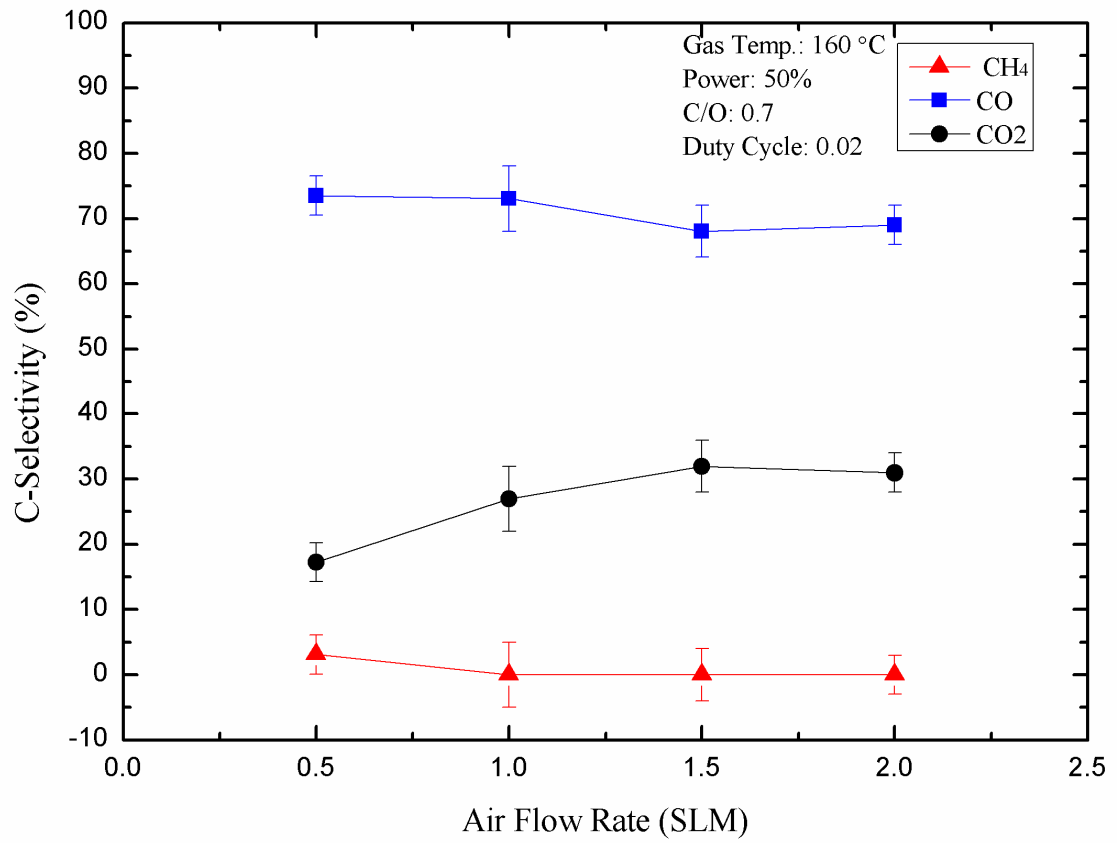
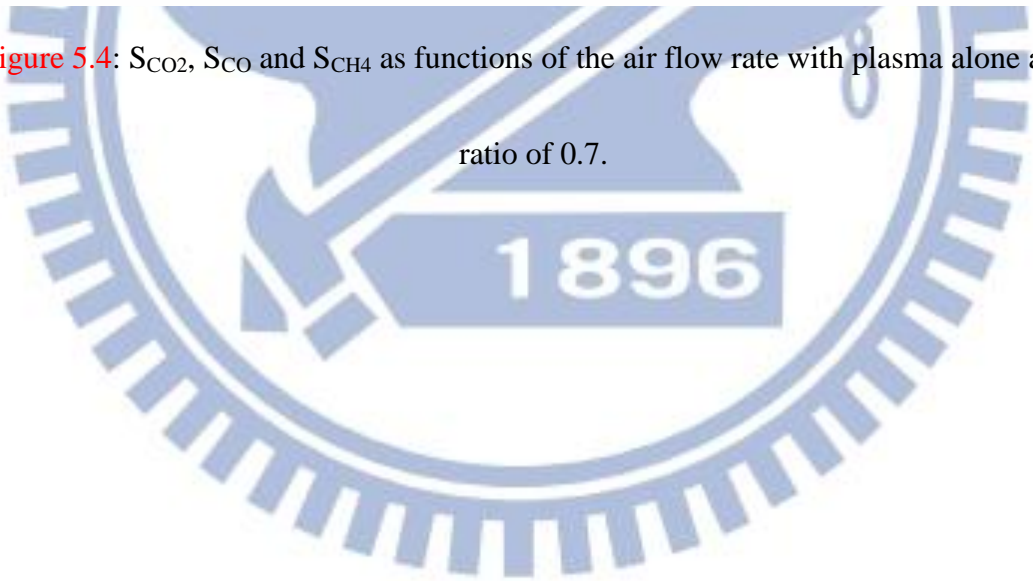
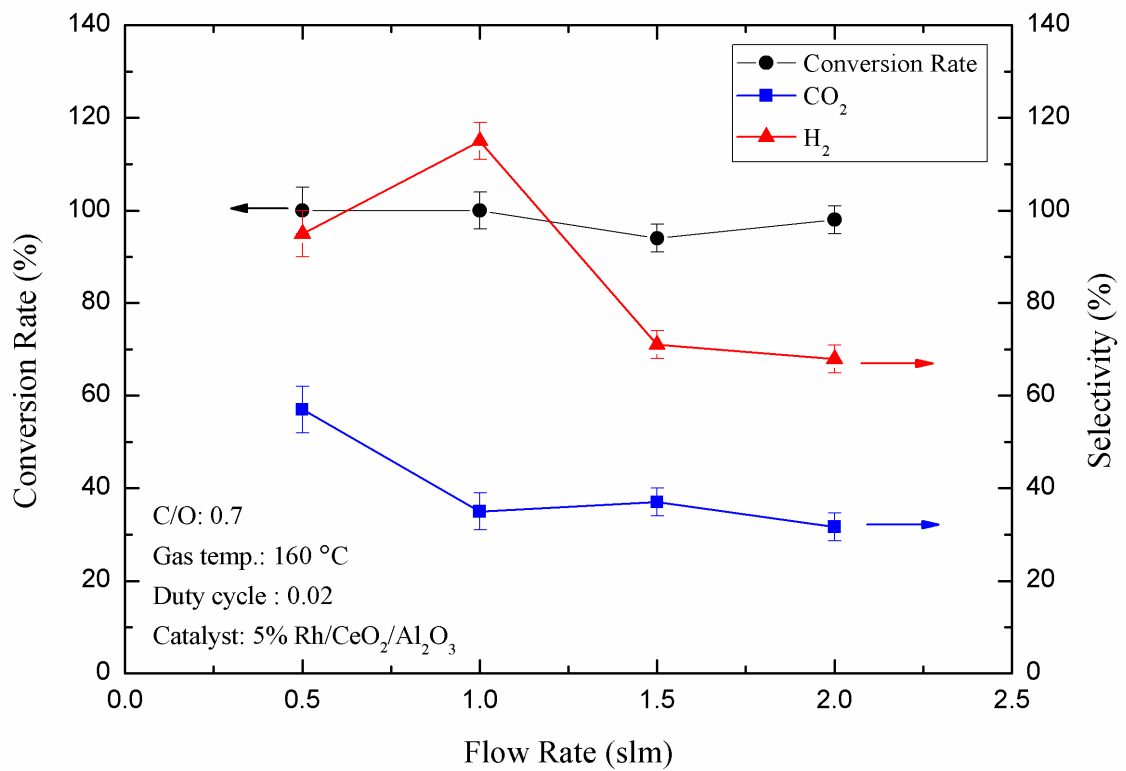
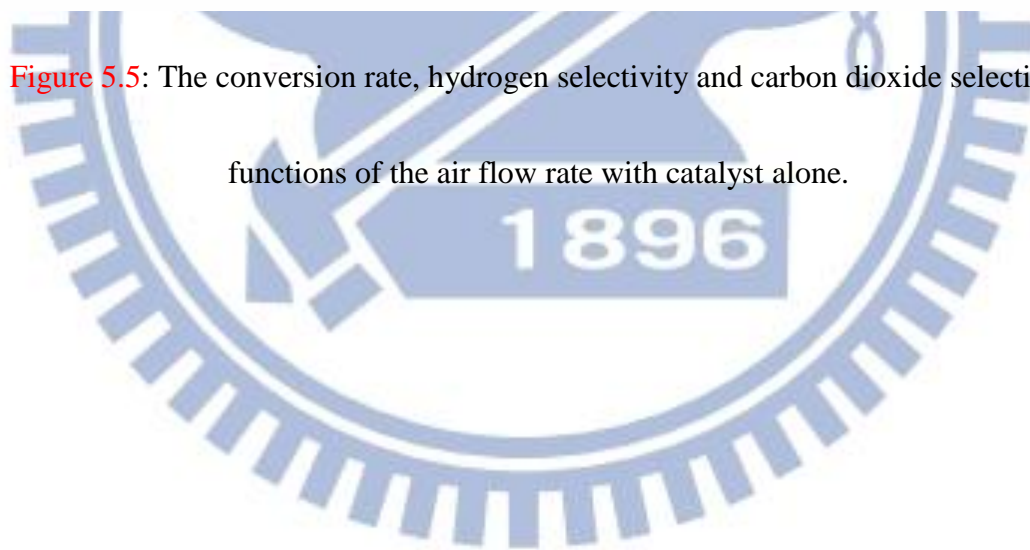


Figure 5.4:  $S_{CO_2}$ ,  $S_{CO}$  and  $S_{CH_4}$  as functions of the air flow rate with plasma alone at a C/O ratio of 0.7.

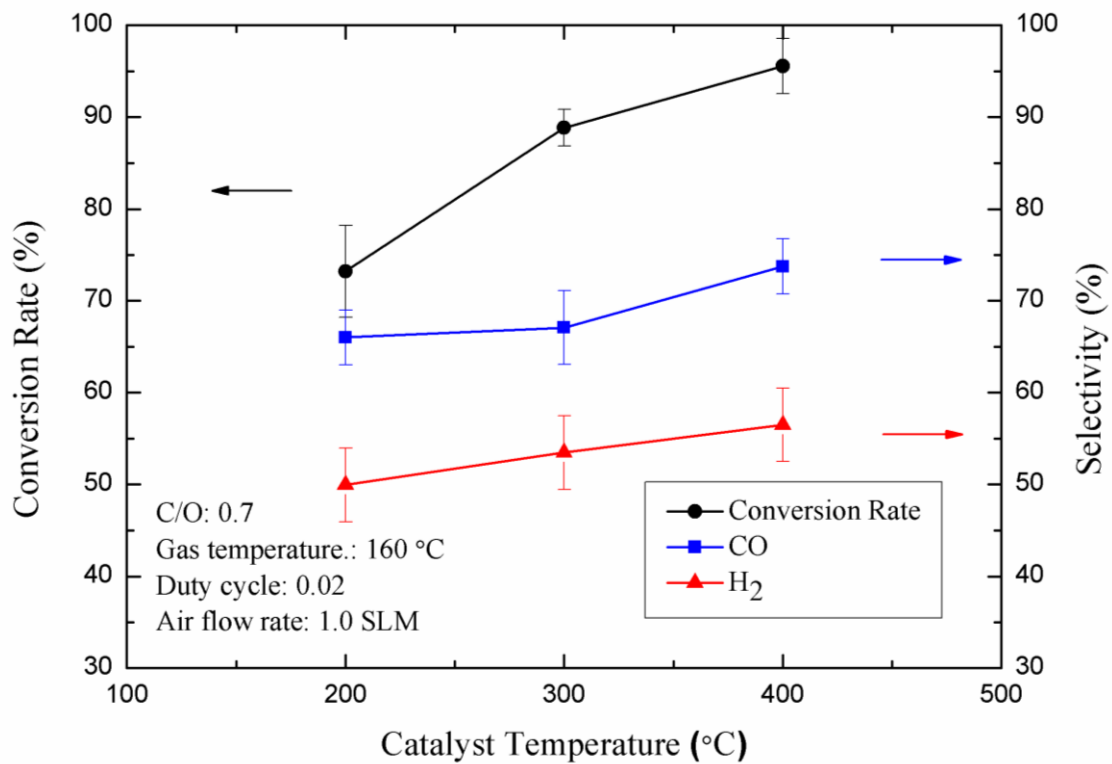




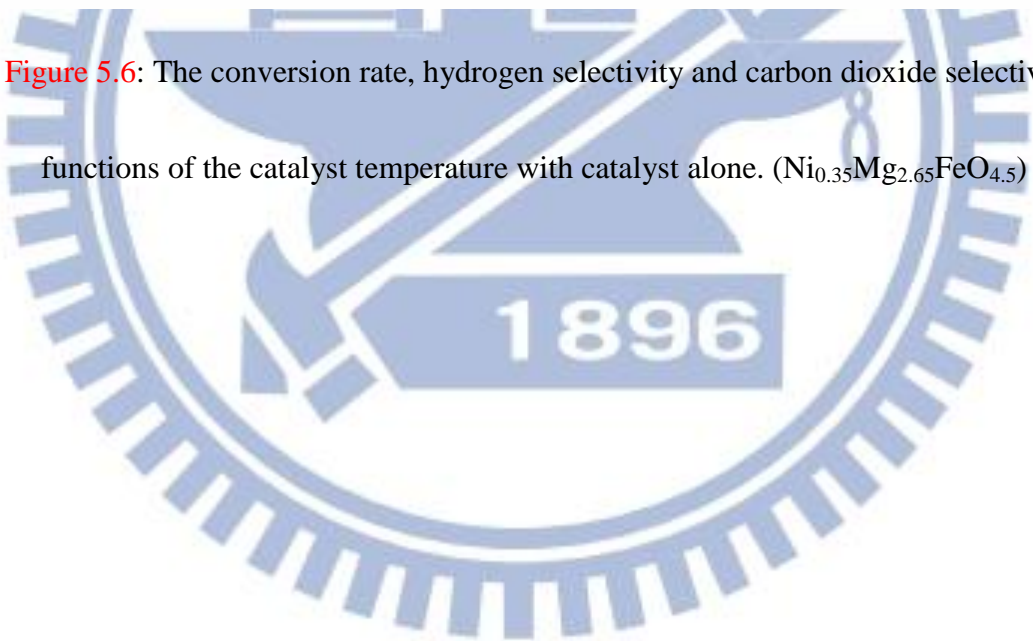
**Figure 5.5:** The conversion rate, hydrogen selectivity and carbon dioxide selectivity as functions of the air flow rate with catalyst alone.

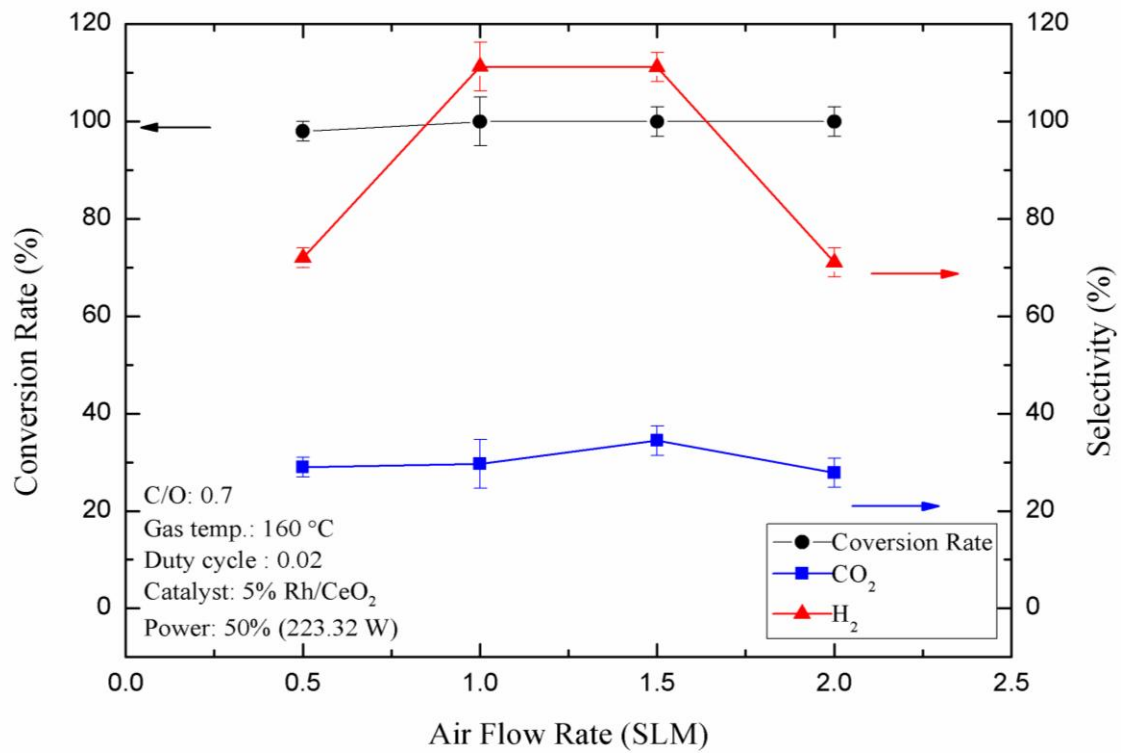




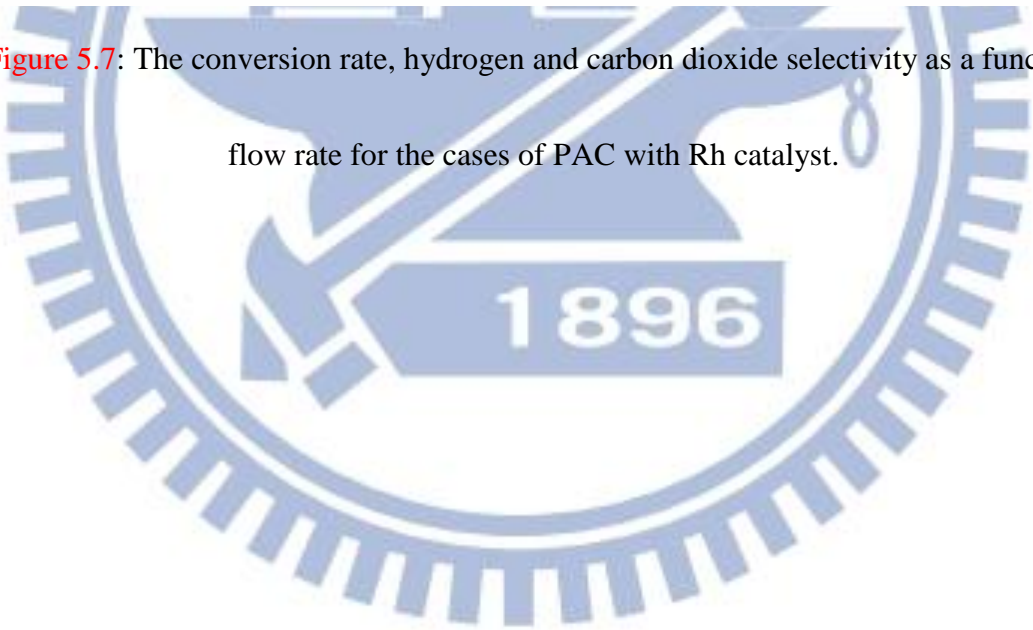


**Figure 5.6:** The conversion rate, hydrogen selectivity and carbon dioxide selectivity as functions of the catalyst temperature with catalyst alone. ( $\text{Ni}_{0.35}\text{Mg}_{2.65}\text{FeO}_{4.5}$ )





**Figure 5.7:** The conversion rate, hydrogen and carbon dioxide selectivity as a function air flow rate for the cases of PAC with Rh catalyst.



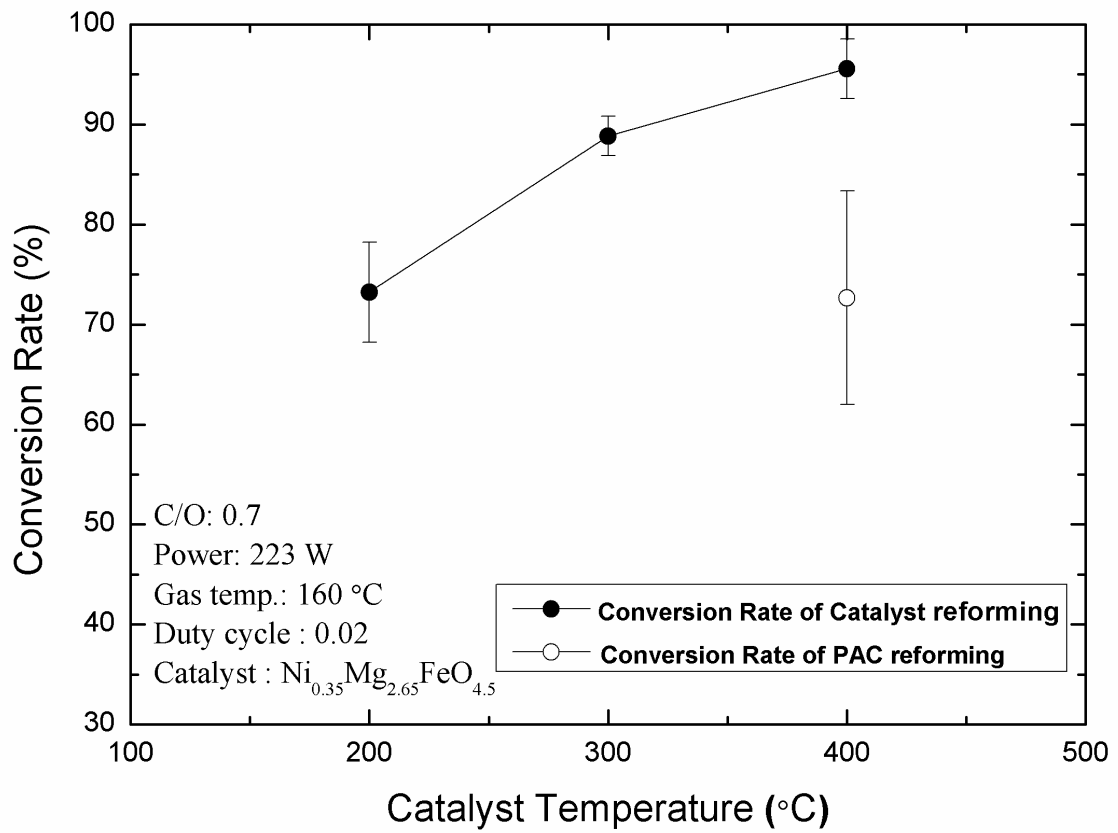


**Figure 5.8:** The comparison of conversion rate between catalyst reforming and PAC reforming using  $\text{Ni}_{0.35}\text{Mg}_{2.65}\text{FeO}_{4.5}$  catalyst.

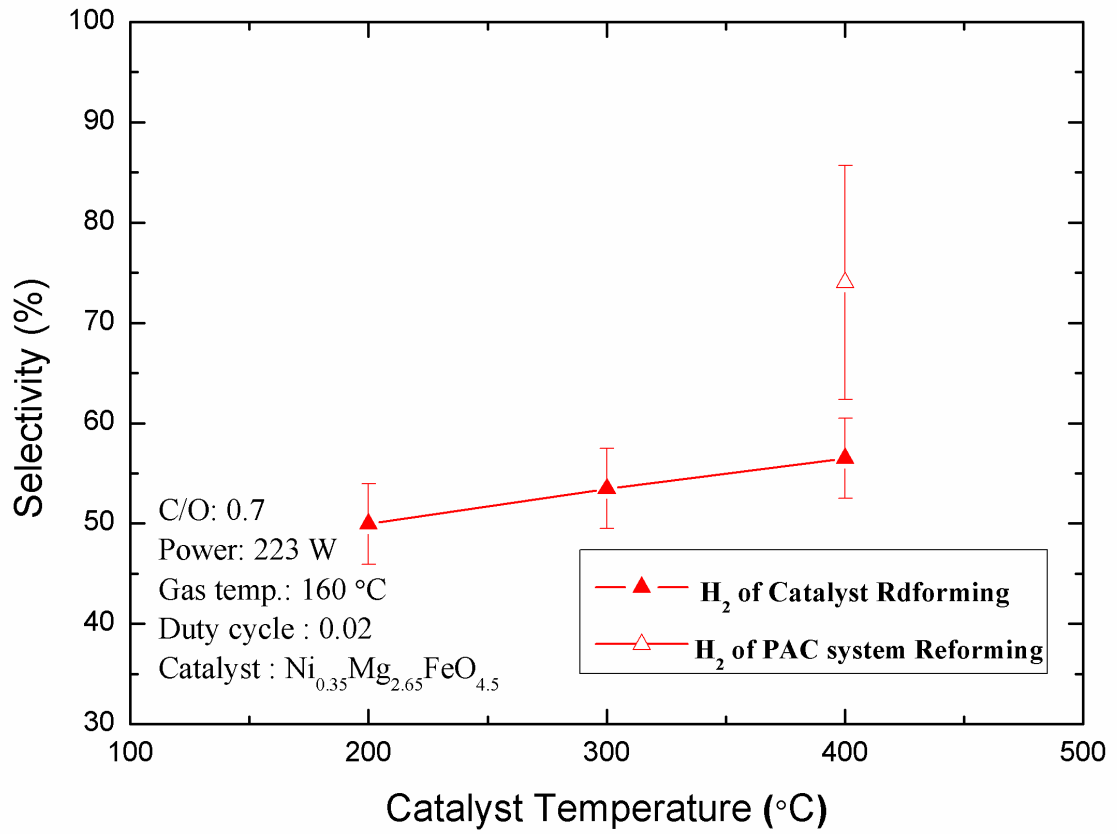


**Figure 5.9:** The comparison of hydrogen selectivity between catalyst reforming and PAC reforming using  $\text{Ni}_{0.35}\text{Mg}_{2.65}\text{FeO}_{4.5}$  catalyst.



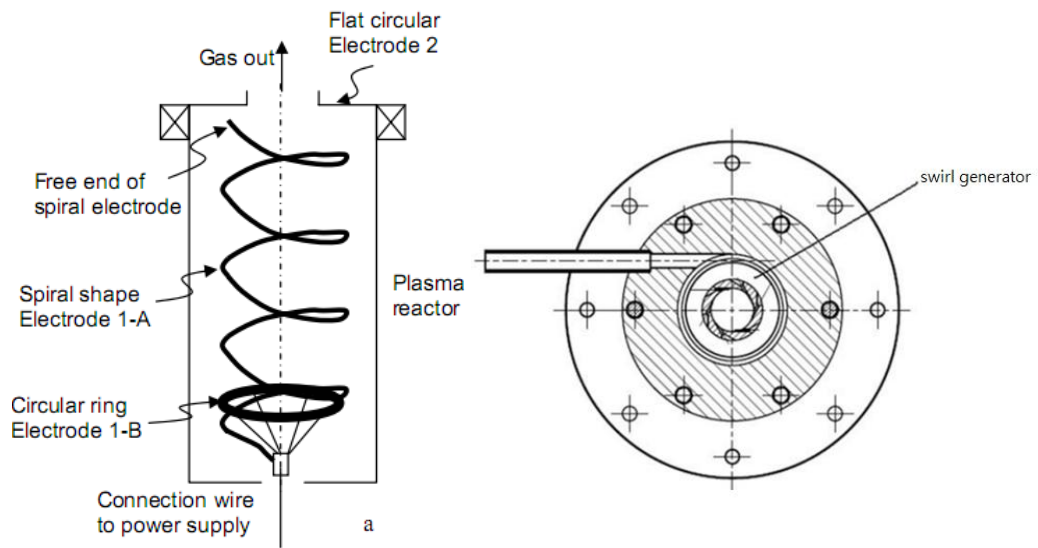
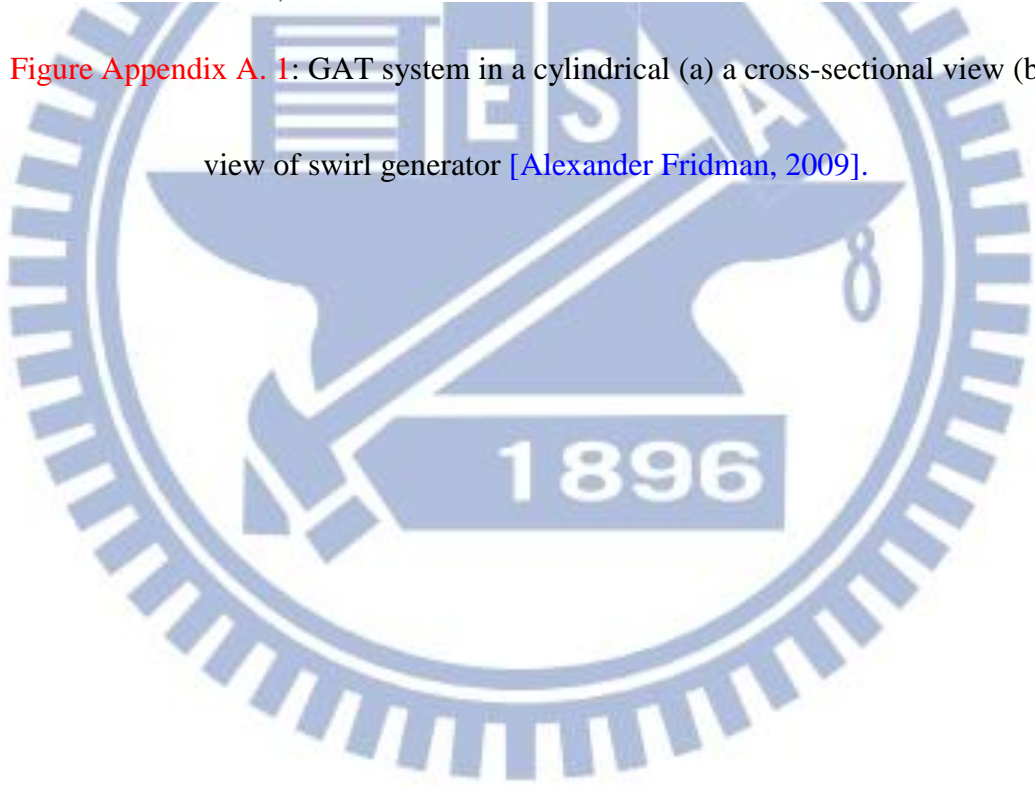
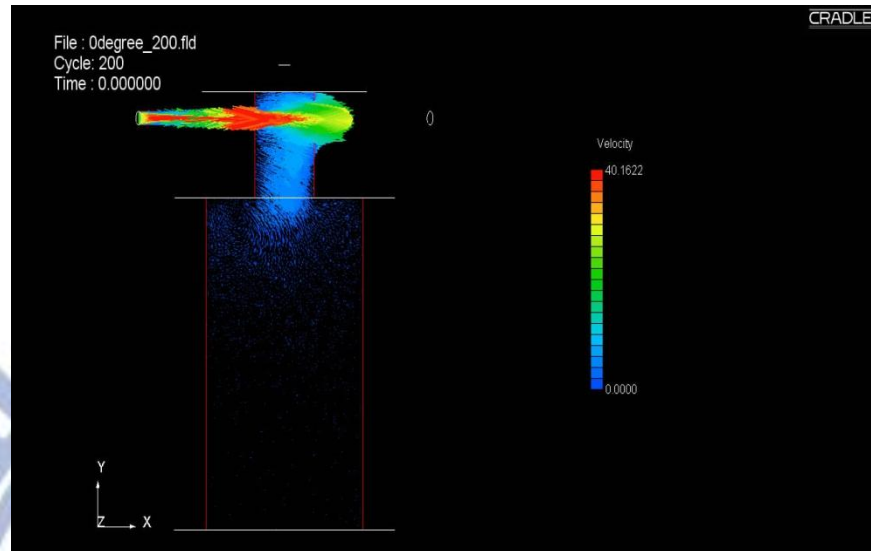


Figure Appendix A. 1: GAT system in a cylindrical (a) a cross-sectional view (b) Top view of swirl generator [Alexander Fridman, 2009].



(a)



(b)

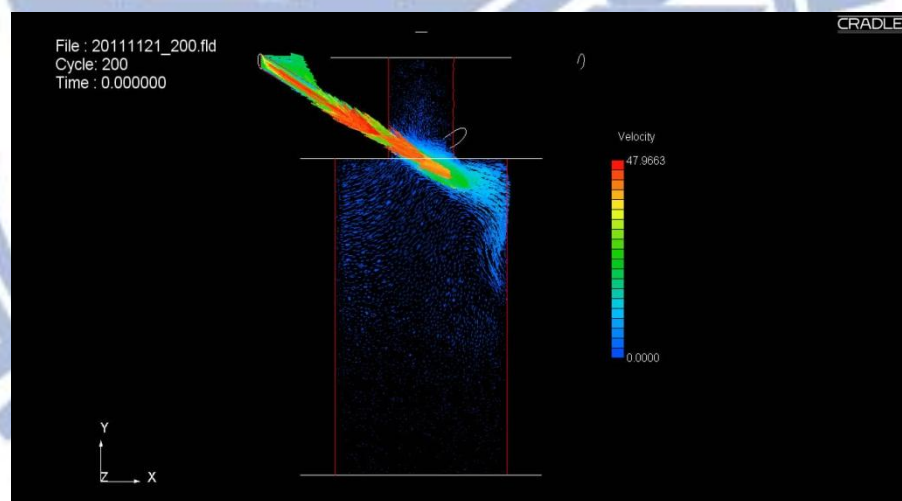


Figure Appendix A. 2: The vector in air flow rate (a). The injection of vector in  $0^\circ$  injected angle (b). The injection of vector in  $30^\circ$  injected angle

- Quartz Diameter = 20 mm
- Inlet Diameter: 2 mm
- Inlet gap: 2 mm
- Outlet Diameter: 1 mm
- Length: 25 mm

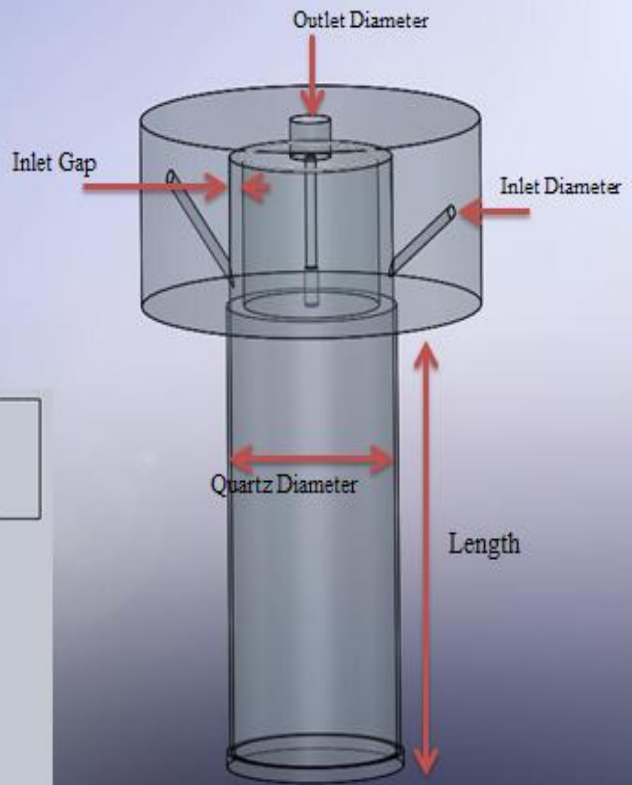
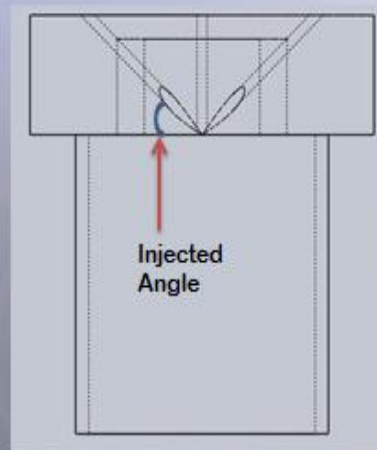


Figure Appendix A. 3: The simulate model in GAT system.

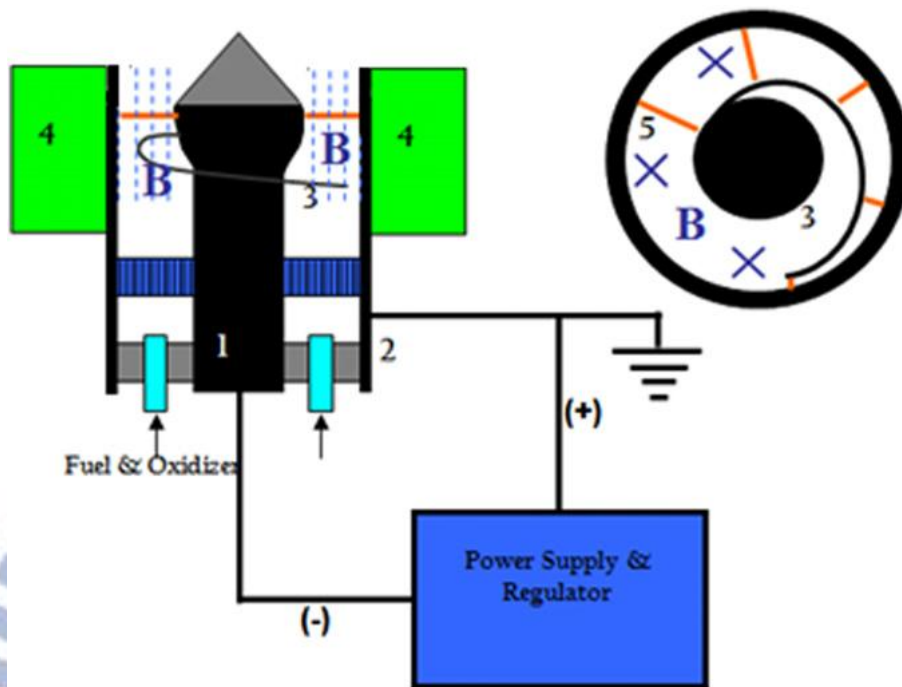
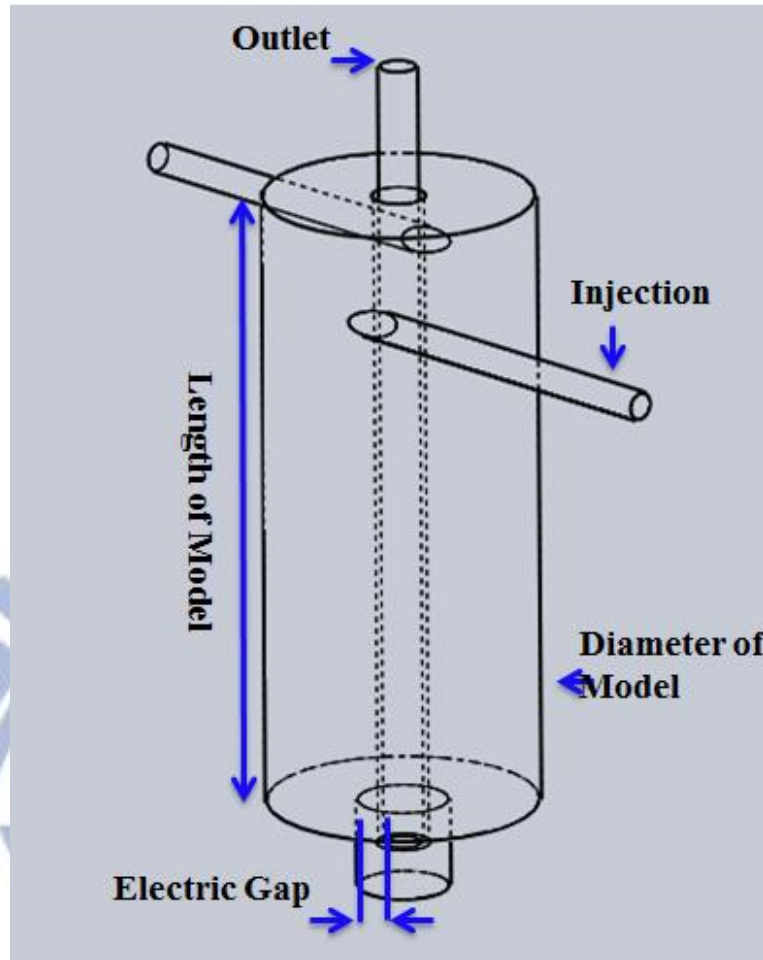


Figure Appendix B. 1: Composition of MGAD system (1) inner electrode (power cathode) (2) outer anodic electrode (ground) (3) wire attached to inner electrode (4) magnet (5) the arc motion between two electrodes [S.P. Gangoli, *et al.*, 2010].





**Figure Appendix B. 3:** The simulate model in MGAD system. Diameter of injection is 2mm; diameter of outlet is 4mm; diameter and length of model is 30mm and 100mm, respectively; and Gap between electrodes is 2mm;

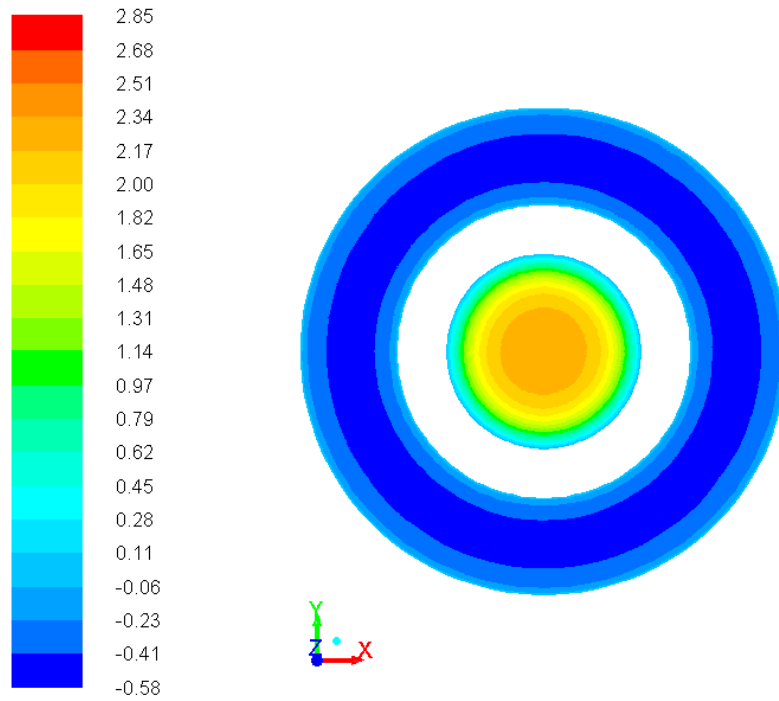


Figure Appendix B. 3: The simulation of MGAD reactor. Flow velocity of z axial direction at the plasma region.

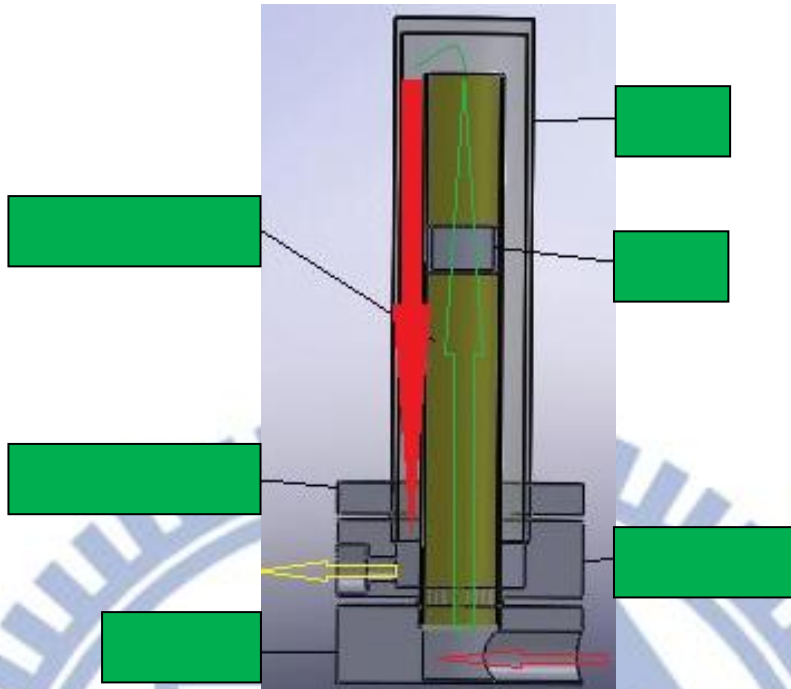


Figure Appendix C. 1: The interior structure of reduction furnace.

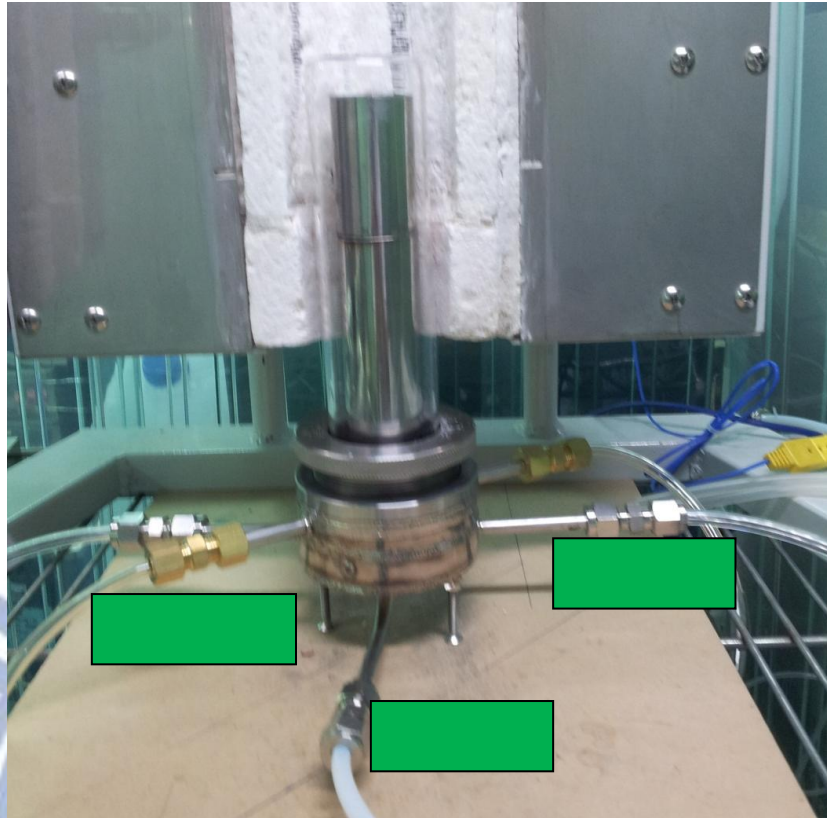


Figure Appendix C. 2: The appearance constructure of reduction furnace.





Figure Appendix C. 3: 10 wt %  $\text{Ni}_{0.35}\text{Mg}_{2.65}\text{FeO}_{4.5}/\text{Al}_2\text{O}_3$  after hydrogen reduction through 5-0.5 hr at the hydrogen flow rates of 50-30 sccm.

